
Reliability-Gated Source Anchoring for Continual Test-Time Adaptation

Vikash Singh¹ Debargha Ganguly¹ Weicong Chen¹ Sabyasachi Sahoo^{2,3}
 Sreehari Sankar¹ Biyao Zhang¹ Mohsen Hariri¹ Shouren Wang¹
 Osama Zafar¹ Christian Gagné^{2,3} Vipin Chaudhary¹

¹Case Western Reserve University ²Université Laval ³Mila - Québec AI Institute
 vikash@case.edu

Abstract

Continual test-time adaptation (CTTA) updates a pretrained model online on an unlabeled, non-stationary stream while anchoring it to a frozen source checkpoint. This anchor is useful only when the source remains reliable. On CCC-Hard, however, a ResNet-50 source falls to approximately 1.3% top-1 accuracy, while existing source-anchored CTTA methods continue applying the same anchor strength. We call this failure mode *blind anchoring* and propose RMEMSAFE, a reliability-gated extension of ROID that uses the frozen source’s normalized predictive entropy to attenuate all explicit source-coupled uses in the objective. When the source posterior approaches uniformity, the gate closes: the source anchor and agreement filter vanish, and the objective reduces to a source-agnostic fallback comprising ROID’s base losses plus marginal calibration. Combined with ASR, RMEMSAFE achieves the lowest error on 8 of 9 matched-split continual-corruption cells and is the best reset-based method on all 9, improving ROID+ASR by 1.05 pp on ResNet-50 and 0.48 pp on ViT-B/16. A controlled source-degradation sweep shows a $1.13\times$ shallower harm slope than ROID+ASR, consistent with the graceful-decay prediction. The entropy gate detects high-entropy source collapse, not confidently wrong low-entropy sources; this scope is explicitly evaluated and discussed.

1 Introduction

A model deployed against a shifting, unlabeled data stream faces a basic safety question: can the adaptation procedure be prevented from driving the model into states worse than those it started in? Continual test-time adaptation (CTTA) addresses this by updating a pre-trained model online while anchoring it to its frozen source [14, 16, 19, 20, 21, 32], the anchor preventing runaway drift under noisy pseudo-labels. The anchor carries a silent, runtime-unchecked precondition: that the source remains a meaningful reference throughout adaptation. On the hardest level of the CCC benchmark [14, 22], the ResNet-50 source’s top-1 accuracy is $\sim 1\%$; yet every prior CTTA method we evaluate continues to pull the adapting model toward this degraded reference with an unconditional ℓ_2 penalty of fixed strength. This blind anchoring is a systematic failure mode of current CTTA methods, and fixed-strength trust in the source can be replaced with a lightweight runtime check that recovers an analytical graceful-decay property.

RMEMSAFE instantiates this check. It gates all explicit source-coupled uses in the ROID [16] optimization: the ℓ_2 anchor toward θ_{src}^* , the cosine-based source-expert agreement filter, and the source-divergence factor inside the anchor. All three are multiplicatively modulated by a single source-reliability scalar $\mathcal{R}_{\text{src}} = \max(0, 1 - \mathcal{H}_{\text{src}})$ derived from source entropy. Because gating alone is not sufficient (the remaining loss must not itself collapse when the gate closes), the gate is composed of three auxiliary stabilizers adapted from standard practice: marginal calibration, a

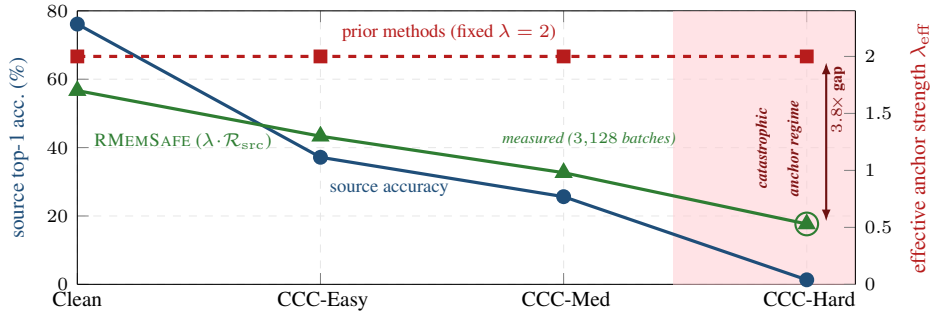


Figure 1: **Continual test-time adaptation under collapsing source reliability.** CTTA anchors the adapter to its frozen source, presuming the source stays a meaningful reference. **Blue:** on CCC, frozen RN-50 source top-1 collapses from 76% (clean ImageNet) to 1.3% (CCC-Hard). **Red dashed:** prior reset-based methods (ROID/ETA/EATA+ASR, ROID+RDumb) hold $\lambda=2$ across all severities, pulling the adapter toward near-noise output. **Green:** RMEMSAFE multiplies λ by the runtime reliability $\mathcal{R}_{src} = \max(0, 1 - \mathcal{H}_{src})$ from the source’s own posterior entropy. The CCC-Hard $\lambda_{eff}=0.53$ is measured (3,128-batch trace, App. Fig. 6); the others follow the monotone entropy-accuracy relation. In the catastrophic regime (shaded), RMEMSAFE attenuates the anchor 3.8 \times ; this attenuation is the analytical safety property demonstrated under controlled degradation (§4, App. M). Matched-split gains on standard CCC reflect the integrated objective; the gate’s safety role is isolated on the controlled source-degradation axis (App. I).

confidence-scaled learning rate, and a decoupled confidence-interpolated flip at inference. The resulting method admits an analytical graceful-decay property (Proposition 1): when source entropy saturates, the source-dependent terms vanish, and the total objective reduces to the base CTTA loss plus the marginal-calibration term, independent of the frozen source parameters. On CCC-Hard, the gate attenuates the runtime anchor by a factor of 3.8 \times relative to prior methods with a fixed $\lambda = 2$. This attenuation is the method’s analytical safety property; its empirical signature is a shallower harm slope under controlled source degradation, while the matched-split benchmark improvements reflect the integrated objective operating jointly.

Two evaluation axes confirm the property. On matched-split evaluations across nine continual-corruption benchmark cells (two architectures, three CCC difficulty levels, two CIN-C orderings, and IN-C 20-revisit), RMEMSAFE achieves the lowest error on 8 of 9 cells, reducing mean CCC error over ROID+ASR, the strongest matched-split prior baseline, by 1.05 pp on ResNet-50 and 0.48 pp on ViT-B/16 (paired t , pooled $p < 10^{-16}$, 95% CI $[-1.16, -0.94]$, Cohen’s $d_z = -3.65$; App. E, Table 7). In a controlled source-degradation experiment that varies clean-test source accuracy from $S=0.75$ down to $S=0.12$ via Gaussian weight noise, RMEMSAFE degrades more gracefully than ROID+ASR across every tested severity, with a harm slope of 11.43 pp per unit of S versus 12.92 pp for ROID+ASR, a 1.13 \times ratio in the direction predicted by Proposition 1.

An explicit scope is stated upfront. The reliability gate uses source *entropy* as its sole reliability signal. This handles the dominant CTTA failure mode observed in practice, high-entropy source collapse as exemplified by CCC-Hard, but not *confidently miscalibrated* sources: a source that is wrong without being uncertain would be deemed reliable by \mathcal{R}_{src} . Designing a correctness-aware reliability signal is a direction for future work (§5). We flag this scope here so the method’s claims are understood narrowly. We confirm this empirically: under a permuted-class low-entropy wrong source RMEMSAFE loses its advantage as predicted, while in the high-entropy regime it preserves it (Table 16). RMEMSAFE is graceful-decay *with respect to entropy-detectable source failure*.

This paper advances graceful-decay CTTA through the following key contributions:

- **Diagnosis of blind anchoring.** On CCC-Hard, prior methods anchor at full strength to a source with $\sim 1\%$ top-1 accuracy: a systematic CTTA failure mode we name and characterize (Figure 1).
- **Reliability-gated CTTA with a graceful-decay guarantee.** To our knowledge, RMEMSAFE is the first CTTA method to gate all explicit source-coupled uses by a runtime reliability signal derived from the frozen source and to admit an analytical graceful-decay property (Prop. 1); the integrated objective keeps the fallback regime well-defined.

- **Empirical confirmation at real and controlled degradation.** 8/9 wins on matched-split benchmarks (per-cell paired t , CIs, d_z in App. E); shallower harm slope than ROID+ASR under a controlled source-quality sweep, within an explicitly stress-tested scope (App. P).
- **Diagnosis of a reset-paradigm failure mode.** On CCC-Hard with ViT-B/16, every reset-based method underperforms non-reset ROID, characterized at matched-split granularity for the first time (§4.3); a reliability-gated τ -sweep partially closes the gap (App. O).

2 Related Work

Test-Time Adaptation. TTA [28] adapts pre-trained models from unlabeled streams via test-time batch-norm recalibration [24], entropy minimization [30], Fisher-regularized updates [19], self-supervised auxiliary updates [15], prototype-based classifier adjustment [10] and per-instance test-time augmentation [36]; non-saturating surrogates, such as the soft likelihood ratio [18] inherited via ROID, replace entropy where it saturates. DeYO [11] shows entropy-based selection fails under disentangled spurious factors, and COME [37] addresses entropy’s overconfidence pathology via Dirichlet-prior conservative entropy. We use entropy as a frozen-source reliability proxy rather than as a self-training target for the adapting expert; this changes the failure mode, but does not eliminate low-entropy miscalibration, which we evaluate in §5 and Appendix P. Standalone TTA still suffers catastrophic forgetting and error accumulation under continuous, non-stationary shifts [13].

Continual Test-Time Adaptation. CTTA stabilizes continuous adaptation through stochastic restoration [32], sample filtering [20], instance-aware normalization under temporal correlation [7, 35], symmetric-cross-entropy mean-teacher training [2] (whose SymCE term we inherit in our source-agnostic fallback), momentum ensembling [16], Kalman filtering [12], memory-efficient self-distilled regularization [27], adaptive collapse-sensing [9], and robust pseudo-labeling self-training [23, 29]. A critical limitation along this line is the implicit assumption that the static source remains a reliable anchor, which fails when severe corruption catastrophically confuses the source. RMEMSAFE addresses this “blind anchoring” flaw by dynamically gating source agreement and anchor strength based on localized source reliability, with an analytically derived graceful-decay property under source collapse.

Long-Term Adaptation and Resets. Long-term severe shifts (e.g., CCC-Hard [17, 22]) cause CTTA models to collapse, motivating the reset paradigm: periodic parameter restoration (RDumb [22]) or adaptive resets (ASR [14]). Resets arrest collapse but may erase acquired target knowledge, and a reset toward a catastrophically confused source can itself be harmful (§4.3). RMEMSAFE is complementary: it attenuates unreliable source-guided updates before they accumulate, improving adaptation-phase stability, and combines effectively with ASR. The CCC and ImageNet-C benchmarks [8, 22] provide the corruption streams used in our evaluation.

3 Method: Reliability-Gated Test-Time Adaptation

When the source posterior is uniform, every source-dependent term should vanish multiplicatively, thereby dropping the source from the gradient (Prop. 1); we now construct the gate and stabilizers that keep this fallback well-behaved.

Let $f_{\theta_{\text{src}}^*}$ denote a pre-trained source model with frozen parameters θ_{src}^* trained on a source distribution \mathcal{D}_S . During continual test-time adaptation, the model observes an unlabeled stream $x_t \in \mathcal{X}_T$ drawn from a shifted, non-stationary target distribution \mathcal{D}_T and continuously updates expert parameters θ_{exp} (initialized as $\theta_{\text{exp}} \leftarrow \theta_{\text{src}}^*$) to minimize empirical risk on the stream. We build on the ROID framework [16], which optimizes a soft-likelihood-ratio loss \mathcal{L}_{slr} and a consistency loss $\mathcal{L}_{\text{cons}}$ on augmented views under diversity and certainty weighting, and additionally anchors the adapting parameters to the frozen source via a fixed-strength ℓ_2 penalty. The design choice that motivates our method is that this anchor strength is *unconditional* on source quality, if the frozen source’s predictions collapse under distribution shift (on CCC-Hard, source top-1 accuracy is approximately 1%), the anchor continues to pull the adapting model toward a useless reference with full strength.

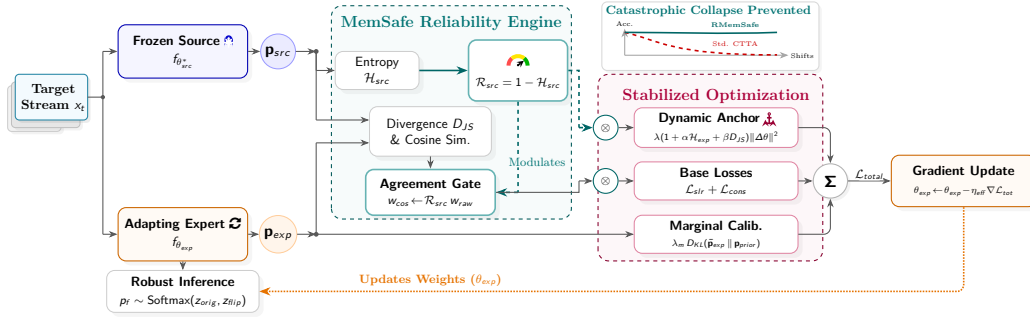


Figure 2: **Overview of RMEMSAFE.** The reliability engine derives the source-reliability gate $\mathcal{R}_{src} = 1 - \mathcal{H}_{src}$ from the frozen source’s entropy. \mathcal{R}_{src} gates all explicit source-coupled uses: the Dynamic Anchor, the agreement filter (interpolating between source agreement and pass-through), and the source-divergence scaling inside the anchor, while leaving the base ROID losses and marginal calibration ungated. At inference, a confidence-interpolated flip average produces the final prediction. When the source collapses, $\mathcal{R}_{src} \rightarrow 0$ and the total loss reduces to a non-collapsing source-agnostic fallback regime (Proposition 1).

The Reliability Gate. For each batch x_t we compute the source and expert predictive distributions $\mathbf{p}_{src} = f_{\theta_{src}^*}(x_t)$ and $\mathbf{p}_{exp} = f_{\theta_{exp}}(x_t)$, and the normalized source entropy

$$\mathcal{H}_{src} = -\frac{1}{\log C} \sum_{c=1}^C p_{src}^{(c)} \log p_{src}^{(c)} \in [0, 1], \quad (1)$$

where C is the number of classes. The *source reliability gate* is $\mathcal{R}_{src} = \max(0, 1 - \mathcal{H}_{src})$. \mathcal{R}_{src} takes value 1 when the source is maximally confident and 0 when its posterior is uniform. RMEMSAFE uses \mathcal{R}_{src} as a single scalar signal to modulate every source-dependent optimization term.

Source-coupled uses gated by reliability. \mathcal{R}_{src} is applied to all explicit places where ROID’s optimization uses source information: the anchor, the agreement filter, and the source-divergence factor inside the anchor. **(i) Divergence-aware dynamic anchor.** Replacing the fixed ℓ_2 penalty of ROID, we define

$$\mathcal{L}_{anch} = \lambda \cdot \mathcal{R}_{src} (1 + \alpha \mathcal{H}_{exp} + \beta D_{JS}(\mathbf{p}_{src} \parallel \mathbf{p}_{exp})) \|\theta_{exp} - \theta_{src}^*\|_2^2, \quad (2)$$

where \mathcal{H}_{exp} is the expert’s normalized entropy, D_{JS} is Jensen–Shannon divergence, and λ, α, β are fixed scalars. The outer \mathcal{R}_{src} prefactor makes the anchor pull toward θ_{src}^* only when the source is reliable; the inner bracket makes the pull stronger when the expert is uncertain or diverges from the source. **(ii) Source-expert agreement gating.** The ROID base losses are gated by a cosine-agreement weight $w_{raw} = w_{min} + (1 - w_{min}) \max(0, \cos(\mathbf{p}_{src}, \mathbf{p}_{exp}))^1$, and the gate itself is gated by \mathcal{R}_{src} :

$$w_{cos} = \mathcal{R}_{src} w_{raw} + (1 - \mathcal{R}_{src}) \cdot 1, \quad (3)$$

which smoothly interpolates between source-expert agreement filtering (when $\mathcal{R}_{src} \rightarrow 1$) and unfiltered adaptation (when $\mathcal{R}_{src} \rightarrow 0$). Under an unreliable source, the agreement signal itself is untrustworthy, so the filter is disabled. **(iii) Divergence-scaled anchor strength.** The βD_{JS} term in (2) is itself source-dependent: a large JS divergence between source and expert carries no information when the source is uninformative. It is gated by the same \mathcal{R}_{src} prefactor via its location inside \mathcal{L}_{anch} , so its contribution decays to zero with source reliability.

Auxiliary Stabilizers for the Fallback Regime. Gating the source-dependent terms is necessary but not sufficient: when $\mathcal{R}_{src} \rightarrow 0$ the gated terms vanish, and the remaining loss must not itself collapse. We therefore include three auxiliary stabilizers, each adapted from standard practice in test-time adaptation. These are not claimed as contributions of this work; we describe them so that the fallback regime is fully specified.

¹ $\max(\cdot, 0)$ is redundant since p_{src}, p_{exp} are softmax outputs and so $\cos \geq 0$; we keep it as a numerical safeguard.

Marginal calibration. To prevent class collapse without enforcing uniform batch marginals, we penalize the KL divergence between the current batch’s class marginal $\bar{\mathbf{p}}_{\text{exp}} = \frac{1}{B} \sum_b \mathbf{p}_{\text{exp},b}$ and an EMA of historical class priors $\mathbf{p}_{\text{prior}}$: $\mathcal{L}_{\text{marg}} = D_{\text{KL}}(\bar{\mathbf{p}}_{\text{exp}} \parallel \mathbf{p}_{\text{prior}})$. This term is not source-dependent and is active regardless of \mathcal{R}_{src} .

Confidence-scaled learning rate. To dampen destructive updates under high expert uncertainty, the effective learning rate is scaled as $\eta_{\text{eff}} = \eta \cdot (\eta_{\text{min}} + (1 - \eta_{\text{min}})(1 - \mathcal{H}_{\text{exp}}))$. This depends on expert uncertainty, not source reliability.

Decoupled flip interpolation at inference. For a test input x_t and its horizontal flip \tilde{x}_t , the final prediction interpolates logits by a confidence-adaptive weight:

$$\mathbf{p}_{\text{final}} = \text{Softmax}((1 - \gamma) z_{\text{orig}} + \gamma z_{\text{flip}}), \quad (4)$$

with $\gamma = \gamma_{\text{min}} + (\gamma_{\text{max}} - \gamma_{\text{min}})(\mathcal{H}_{\text{exp}}(z_{\text{orig}}))$. Confident predictions are dominated by the original view; uncertain predictions benefit from the augmented view.

Total Objective and Graceful Decay. The total training objective is

$$\mathcal{L}_{\text{total}} = w_{\text{cos}}(\mathcal{L}_{\text{slr}} + \mathcal{L}_{\text{cons}}) + \lambda_{\text{marg}} \mathcal{L}_{\text{marg}} + \mathcal{L}_{\text{anch}}. \quad (5)$$

The design is structured so that the novel mechanism, reliability gating, has a well-defined limiting behavior.

Proposition 1 (Graceful decay under source collapse). *When the source posterior becomes uniform, $\mathcal{H}_{\text{src}} \rightarrow 1$ implies $\mathcal{R}_{\text{src}} \rightarrow 0$. Under this limit: (i) $\mathcal{L}_{\text{anch}} \rightarrow 0$, so the ℓ_2 anchor toward θ_{src}^* is completely removed; (ii) $w_{\text{cos}} \rightarrow 1$, so the source-expert agreement filter reverts to an unfiltered pass-through; (iii) the total objective reduces to $\mathcal{L}_{\text{slr}} + \mathcal{L}_{\text{cons}} + \lambda_{\text{marg}} \mathcal{L}_{\text{marg}}$, which is independent of θ_{src}^* and well-defined.*

proof. Substituting $\mathcal{R}_{\text{src}} = 0$ into Eq. (2) zeroes the outer prefactor of the anchor loss, so $\mathcal{L}_{\text{anch}} = 0$ regardless of the value of $\|\theta_{\text{exp}} - \theta_{\text{src}}^*\|_2^2$ and regardless of the inner divergence and entropy terms; the ℓ_2 pull toward θ_{src}^* is therefore removed, not merely attenuated. Substituting $\mathcal{R}_{\text{src}} = 0$ into Eq. (3) yields $w_{\text{cos}} = 0 \cdot w_{\text{raw}} + (1 - 0) \cdot 1 = 1$, so the source-expert agreement filter reverts to an unfiltered pass-through. Substituting both into Eq. (5) gives $\mathcal{L}_{\text{total}} = \mathcal{L}_{\text{slr}} + \mathcal{L}_{\text{cons}} + \lambda_{\text{marg}} \mathcal{L}_{\text{marg}}$, which depends only on the expert predictions \mathbf{p}_{exp} and the running marginal $\mathbf{p}_{\text{prior}}$, and is therefore independent of θ_{src}^* .

Proposition 1 states the load-bearing property of the method: in the limit of a catastrophically confused source, RMEMSAFE does not enforce a corrupted prior; instead, it reduces to a source-agnostic adaptation regime comprising the ROID base losses plus a marginal-calibration term. The confidence-LR and decoupled flip remain active throughout the regime because they depend on expert rather than source statistics.

Scope of Proposition 1. The proposition concerns only the regime in which source entropy is *high*. It does not claim the gate detects all forms of source failure; in particular, a source that is *confidently wrong* has low entropy and would be deemed reliable by \mathcal{R}_{src} . We return to this scope boundary in §5. The per-batch update combining equations (3)–(5) with the ASR adaptive-selective reset controller [14] is given as Algorithm 1 in Appendix A. Hyperparameters are fixed across all nine benchmark cells; specific values are in Table 3 of Appendix B.

4 Experiments

4.1 Experimental Setup

Benchmarks. We evaluate on three continual-TTA benchmark families. **CCC** [22] is a non-stationary ImageNet-scale stream of continuously transitioning corruptions; we use the three difficulty levels of Lim et al. [14] (*Easy, Medium, Hard*; source accuracies $\sim 34\%$, 17% , 1%), each over 9 split seeds of 50,000 samples. **CIN-C** (CIFAR-10-C, 20 revisits) cycles 15 corruptions $20\times$; we report i.i.d. and correlated (Dirichlet $\alpha=0.1$) orderings over 10 seeds. **IN-C** is the analogous ImageNet-C 20-revisit protocol. These nine cells span two architectures (ResNet-50, ViT-B/16). The CCC and IN-C cells use ImageNet-pretrained ResNet-50 and ViT-B/16; the CIN-C cells follow the standard CIFAR-10-C protocol with a CIFAR-10-trained WRN-28-10 backbone (App. L). §4.4 adds a controlled *source-degradation* experiment that varies clean-test source accuracy via Gaussian weight noise, probing Proposition 1’s graceful-decay regime directly.

Table 1: Error (% , lower is better) on all nine continual TTA benchmark cells, means across 9 CCC splits, 10 CIN-C seeds, or a single IN-C 20-revisit run; per-split std in Table 4 (appendix). **Bold** marks the best method per column. All baselines are re-run locally on identical data splits. Our method (grey row) wins 8 of 9 cells; the single non-win (CCC-Hard ViT) is analyzed in §4.3.

Method	CCC ResNet-50			CCC ViT-B/16			Long-horizon continual		
	Easy	Med.	Hard	Easy	Med.	Hard	CIN _{iid}	CIN _{corr}	IN-C
Source	62.83	74.35	98.67	41.72	51.44	86.58	81.85	81.85	96.42
ROID	47.61	54.24	86.07	36.56	42.69	75.98	51.29	51.74	61.45
ROID+RDumb	47.78	54.52	86.77	36.80	43.06	76.50	51.86	52.30	62.27
ETA+ASR	46.70	53.58	89.74	41.18	45.93	80.11	52.62	53.02	65.30
EATA+ASR	46.71	53.62	88.89	41.18	45.93	80.58	52.60	53.00	63.11
ROID+ASR	46.46	52.80	84.56	36.47	41.72	84.04	50.37	50.72	58.13
RMEMSAFE, no ASR	46.80	53.73	86.60	37.37	43.86	76.36	51.54	51.92	62.30
RMEMSAFE+ASR (ours)	45.27	51.62	83.81	35.97	41.66	83.18	49.49	49.92	57.66

Baselines. We compare against seven baselines, all re-run locally on identical splits for matched comparison: *Source* (frozen, no adaptation); *ROID* [16], the strongest soft-weighting CTTA method; *ROID+RDumb* [22], adding periodic hard reset every 1,000 updates; *ETA+ASR*, *EATA+ASR* [14, 19], combining entropy-filtered adaptation with Adaptive And Selective Reset; *ROID+ASR* [14], the strongest prior reset baseline in our matched reruns; and *RMEMSAFE-noASR*, our gate without reset to isolate the gating contribution. On our shards, *ROID+ASR*’s CCC-Hard error differs from the streamed-data number in Lim et al. [14] by ~ 7 pp; the offset is approximately constant across methods and preserves ranking (Appendix Q), so we evaluate all methods on the same shards.

Implementation. We use ResNet-50 and ViT-B/16 backbones with publicly released ImageNet weights. Following *ROID*, we adapt only the affine parameters of normalization layers using SGD (learning rate 2.5×10^{-4} , momentum 0.9, batch size 64, no weight decay). *RMEMSAFE* introduces five additional hyperparameters, all fixed across all nine benchmarks: anchor strength $\lambda=2.0$, entropy scale $\alpha=2.0$, divergence scale $\beta=1.0$, marginal weight $\lambda_{\text{marg}}=0.1$, and confidence-LR floor $\eta_{\text{min}}=0.2$.

4.2 Matched-Split Benchmark Results

RMEMSAFE+ASR achieves the lowest error on **8 of 9** benchmark cells (Table 1) and is the *uniquely best method in the reset-based family on every one of the 9 cells*; the single exception (CCC-Hard ViT, against non-reset *ROID*) is a property of the reset paradigm itself, which we analyze in §4.3. Against *ROID+ASR*, the strongest matched-split prior baseline, *RMEMSAFE* reduces the CCC-ResNet-50 mean by **1.05 pp** and the CCC-ViT mean by **0.48 pp**. On the long-horizon benchmarks, where twenty revisit cycles amplify error accumulation, *RMEMSAFE* reduces CIN-C error by 0.80 to 0.88 pp and IN-C error by 0.47 pp relative to *ROID+ASR*. No other baseline, including *ETA+ASR* and *EATA+ASR*, achieves the best score on any cell. Per-split paired *t*-tests (Appendix E) confirm the ResNet-50 improvements are statistically significant: the pooled comparison across the three CCC levels yields $p < 10^{-16}$ against *ROID+ASR*. The pooled CCC RN-50 effect is $\Delta = -1.05$ pp, 95% CI $[-1.16, -0.94]$, $d_z = -3.65$ (Table 7); CIN-C cells all significant at $p < 10^{-10}$. The lone non-significant cell (CCC-Hard ViT, $p=0.052$) is the reset-paradigm failure of §4.3.

Adaptation-gap decomposition. The sequential progression from *Source* to *RMEMSAFE+ASR* decomposes the total CCC ResNet-50 improvement into three stages:

$$\underbrace{78.62}_{\text{Source}} \xrightarrow{-15.98} \underbrace{62.64}_{\text{ROID}} \xrightarrow{-1.36} \underbrace{61.28}_{\text{ROID+ASR}} \xrightarrow{-1.05} \underbrace{60.23}_{\text{RMEMSAFE+ASR}} \quad (\text{pp CCC-mean}) \quad (6)$$

Pure adaptation contributes the bulk of the gain (15.98 pp), ASR reset contributes a further 1.36 pp, and the integrated *RMEMSAFE* objective contributes another 1.05 pp on top of *ROID+ASR*. As shown in Eq. 6, decomposing this final 1.05 pp by component (detailed in App. J) attributes ~ 1.00 pp to the auxiliary stabilizers (decoupled flip, confidence-scaled LR, marginal calibration) and ~ 0.04 pp to the reliability-gated terms (anchor, source-expert agreement) on the CCC mean. This decomposition reflects the runtime regime: the matched-split gains come from the integrated objective, while the

Table 2: **CCC ViT-B/16 accuracy (%)** across difficulty levels, focused view of the reset-paradigm observation. Plain ROID (no reset) leads on Hard because resets toward the degraded source are harmful in this regime. Among reset-based methods, RMEMSAFE+ASR is best on Easy and Medium and best within the reset-based family on Hard. **Bold** marks the best per column.

Method	Easy	Med.	Hard
Source	58.28	48.56	13.42
ROID [16]	63.44	57.31	24.02
<i>Reset-based methods</i>			
ROID + RDumb [22]	63.20	56.94	23.50
ETA + ASR [14, 19]	58.82	54.07	19.89
EATA + ASR [14, 19]	58.82	54.07	19.42
ROID + ASR [14]	63.53	58.28	15.96
RMEMSAFE+ASR (Ours)	64.03	58.34	16.82

gate’s safety role is isolated on the controlled source-degradation axis below and by the confidently-wrong-source stress test (App. P).

Head-to-head against reset-based methods. Across the 9 benchmark cells, RMEMSAFE+ASR never loses to any of the three ASR-augmented baselines (ETA+ASR, EATA+ASR, ROID+ASR) or to ROID+RDumb: 9 / 9 wins in the reset-based family.

4.3 Reset-Paradigm Failure on ViT-Hard

Our matched-split evaluation surfaces a regime in which every reset-based method we evaluate underperforms the non-reset ROID baseline. On CCC-Hard with ViT-B/16, the strict ordering,

$$\underbrace{75.98}_{\text{ROID}} < \underbrace{76.50}_{\text{ROID+RDumb}} < \underbrace{80.11}_{\text{ETA+ASR}} \approx \underbrace{80.58}_{\text{EATA+ASR}} < \underbrace{83.18}_{\text{RMEMSAFE+ASR}} < \underbrace{84.04}_{\text{ROID+ASR}} .$$

is invariant across base adapters (ROID, ETA, EATA, RMEMSAFE) and reset mechanisms (periodic, adaptive). The phenomenon is specific to ViT-B/16: on the same CCC-Hard benchmark with ResNet-50 the same ASR controller improves on plain ROID by 1.51 pp (84.56 vs 86.07), even though the ResNet-50 source is harder (1.33% top-1 versus 13.42% on ViT). Source quality alone, therefore, does not explain the ordering; if it did, the ResNet-50 reset configuration should suffer at least as much. Plausible architecture-specific candidates include attention-block sensitivity to discrete parameter restoration and LayerNorm-affine dynamics under repeated resets, but our experiments do not isolate a single mechanism, and we report this as a characterized observation rather than a fully explained one. Within the reset-based family, RMEMSAFE+ASR is the strongest on CCC-Hard ViT, improving over ROID+ASR by 0.86 pp; gating the reset trigger itself by a time-averaged \mathcal{R}_{src} (App. O) closes most of the residual gap to non-reset ROID at threshold $\tau_{\text{gate}} = 0.40$, recovering the non-reset baseline on the mean (76.42 vs 75.98). A full mechanistic account of the architecture-specific failure and a reset controller that is reliable for every split rather than the mean are left to future work (§5).

4.4 Controlled Source Degradation

The main benchmark results establish that RMEMSAFE improves over prior methods on standard continual-corruption streams, but they do not directly measure how the method responds to *varying* source quality, the axis along which Proposition 1 makes its prediction. To probe this axis, we conduct a controlled experiment in which the source model’s clean-test accuracy is varied continuously by injecting Gaussian noise into its convolutional weights and normalization affine parameters. For each parameter tensor θ_k with per-tensor standard deviation σ_k , we set $\theta_k \leftarrow \theta_k + \epsilon \sigma_k \mathcal{N}(0, I)$, with ϵ calibrated by binary search so that the resulting source has clean-test accuracy $S \in \{0.75, 0.30, 0.12\}$. Biases and BN running statistics are not perturbed. Full protocol is in Appendix L. We then run ROID+ASR and RMEMSAFE+ASR on CIN-C (both i.i.d. and correlated orderings, 3 seeds) using each of the three degraded sources, for a total of 36 runs. Figure 3 reports the result.

Interpretation. RMEMSAFE+ASR is better than or tied with ROID+ASR on all 6 cells and strictly better on 5 (at $S=0.75$ correlated the pooled gap is +0.29 pp; within-cell std on this configuration is 0.34 for ROID+ASR and 0.40 for RMEMSAFE+ASR, both larger than the observed gap, so we treat

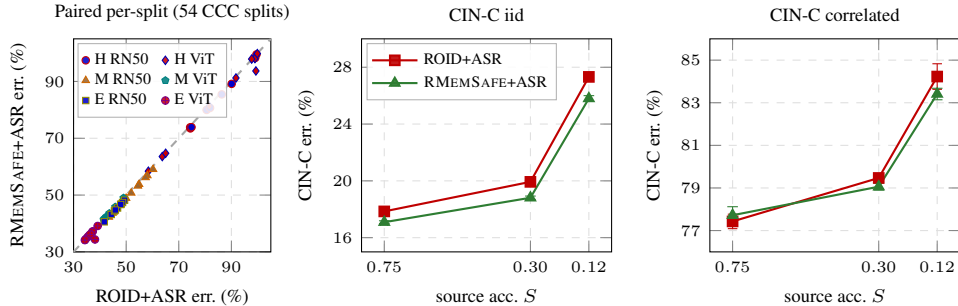


Figure 3: **Left:** paired per-split CCC comparison ($n=54$); RMEMSAFE is below $y=x$ on 51 splits, on the diagonal ($|\Delta| \leq 0.02$ pp) on 2, and 0.17 pp above on 1 (a CCC-Hard ViT split where both methods are at $\sim 98\%$ error). **Center, right:** controlled source-degradation on CIN-C, varying source clean-test accuracy S via Gaussian weight noise (Appendix L). Error bars: ± 1 std over 3 seeds; x-axis reversed. The RMEMSAFE+ASR – ROID+ASR gap widens monotonically as S decreases (§4.4), consistent with graceful decay.

this cell as a tie). The gap widens monotonically as S decreases, at $S=0.75$ the pooled improvement is -0.23 pp; at $S=0.30$, -0.76 pp; at $S=0.12$, -1.17 pp. Fitting a harm slope $H_m = (\text{err}_m(S_{\min}) - \text{err}_m(S_{\max})) / (S_{\max} - S_{\min})$ across the tested range yields $H_{\text{ROID+ASR}} = 12.92$ pp per unit of S versus $H_{\text{RMEMSAFE+ASR}} = 11.43$, a ratio of 1.13 in the direction predicted by Proposition 1. Per-batch reliability traces collected during these runs show \mathcal{R}_{src} drifting monotonically from approximately 0.84 at $S=0.75$ to approximately 0.78 at $S=0.12$ (Appendix L, Table 13). The drift is modest because weight noise does not push the source to the posterior-uniform limit that saturates the gate, but it is consistent across seeds and both orderings, confirming that the gate is tracking source quality rather than collapsing to a constant.

Scope. Weight noise yields uniformly-confused, high-entropy sources, directly probing the regime \mathcal{R}_{src} is designed to detect; low-entropy miscalibration is not exercised here (§5).

4.5 Ablations

To isolate each component of the RMEMSAFE objective, we disable one contribution at a time and re-evaluate on all 27 CCC ResNet-50 splits. Figure 4 shows the degradation of CCC-mean error.

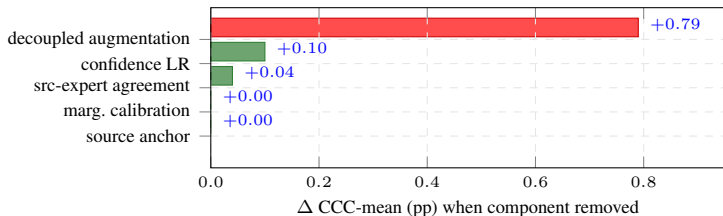


Figure 4: **Component ablation on CCC ResNet-50** (mean over 27 splits). Two of the five ablated components (anchor, source-expert agreement) are multiplied by $\mathcal{R}_{\text{src}} \approx 0.26$ at CCC-Hard runtime (App. K); the three ungated components (marg. calibration, confidence-scaled LR, decoupled flip) are not. The decoupled flip is the only contribution with a large leave-one-out effect (+0.79 pp).

Gated components interpretation. Figure 4 shows that several leave-one-out effects are small on the standard CCC mean. This is the expected runtime behavior of reliability gating, and is directly predicted by Proposition 1. Recall from Eq. (2) that the source anchor, the source-expert agreement gate, and the divergence term are all multiplied by $\mathcal{R}_{\text{src}} = \max(0, 1 - \mathcal{H}_{\text{src}})$. On CCC-Hard, the frozen source produces a broad low-confidence posterior (top-1 accuracy about 1%, normalized entropy $\mathcal{H}_{\text{src}} \approx 0.74$), so \mathcal{R}_{src} stabilizes at a low floor of roughly 0.26 for the entire run rather than collapsing to zero (Figure 6, appendix). Consequently, $\mathcal{L}_{\text{anch}}$ is scaled down by roughly $3.8\times$ at runtime relative to its configured strength, the same $3.8\times$ attenuation previewed in Figure 1, and at this effective strength the anchor contributes a small but non-zero pull. The matched-split gains

therefore come from the integrated objective, while the gate’s safety role is isolated on the controlled source-degradation axis in §4.4. Separately, a $16\times$ sweep of λ (Figure 5) moves CCC-Hard error by only 0.21 pp, because every configured λ is multiplied by the same ~ 0.26 factor at runtime, so the effective sweep range is narrow. Under catastrophic shifts, the system gracefully attenuates the source-anchored terms, and the residual objective is borne by the ROID base losses, marginal calibration, and the decoupled inference-time flip, in the non-collapsing fallback regime of Proposition 1.

4.6 Robustness Analysis

Split-level paired comparison. Figure 3 plots per-split ROID+ASR error against RMEMSAFE+ASR error on all 54 CCC splits. Every point except three lies below the $y=x$ diagonal: RMEMSAFE reduces error on 51 of 54 individual splits, is essentially on the diagonal on 2, and is 0.17 pp above it on 1. All three near-diagonal points are CCC-Hard ViT splits on which both methods are pinned near chance accuracy ($\sim 98\%$ error); the single marginal non-improvement at that accuracy level is not distinguishable from seed noise. The clear diagonal shift on the remaining 51 splits demonstrates that the mean improvements in Table 1 are consistent across individual splits rather than artifacts of favorable averaging.

Variance across splits. Per-split standard deviations on CCC-Hard (ResNet-50) are ± 9.52 pp for RMEMSAFE+ASR and ± 9.39 pp for ROID+ASR, a property of the benchmark rather than of either method: both vary by similar amounts across the *same* splits, so the paired comparison of Figure 3 and the matched-split means of Table 1 are more informative than any single-split number.

Within-run behavior. On CCC-Hard split 3 with RN-50, sliding-window accuracy (window= 400, stride= 30) over 3,128 batches shows RMEMSAFE+ASR holds a 1.1 pp higher mean band than ROID+ASR (27.2% vs. 26.1%), with smaller dips around reset events; full trace in Appendix K.

Local-data offset. Our CCC shards yield numbers ~ 7 pp harder than the streamed data of Lim et al. [14] on CCC-Hard (RN-50); the offset is approximately constant across methods and preserves ranking (Appendix Q). Cross-study absolute comparisons on CCC-Hard should therefore be interpreted with caution, but the matched-split head-to-head of Table 1 is the unbiased estimator of relative method quality.

5 Discussion

Our matched-split evaluation surfaces two scope boundaries that frame the contribution. First, the *reset paradigm itself* has a boundary distinct from any particular schedule: on CCC-Hard with ViT-B/16, every reset-based CTTA method we evaluate underperforms non-reset ROID across base adapters (ROID, ETA, EATA, RMEMSAFE) and reset mechanisms (periodic, adaptive); all of them restore (in a harmful way) parameters toward a degraded frozen source. The failure is inherent to the design pattern rather than timing, and to our knowledge has not been characterized at matched-split granularity before; a direct extension is to gate the reset trigger itself by a time-averaged \mathcal{R}_{src} , suppressing resets toward a source already deemed unreliable by the same signal that gates the adaptation loss. Second, reliability gating must not be conflated with reliability *detection*: the gate uses source entropy as its sole signal, which keeps Proposition 1 analytically available and is correct for high-entropy source collapse (on CCC-Hard ResNet-50, $\mathcal{H}_{\text{src}} \approx 0.74$ closes the gate to $\mathcal{R}_{\text{src}} \approx 0.26$, attenuating the anchor by $3.8\times$), but a *confidently miscalibrated* source (low entropy on wrong classes) would be deemed reliable and the anchor activated toward it. Standard CTTA benchmarks produce high-entropy collapse rather than low-entropy miscalibration, so this regime is not exercised by the main benchmark but is a real failure mode in principle; the entropy-based gate is sound under the typical-shift assumption that catastrophic failure manifests as predictive uncertainty, and a correctness-aware signal preserving the graceful-decay guarantee is a direction for future work.

6 Conclusion

RMEMSAFE gates all explicit source-coupled uses in the CTTA objective by $\mathcal{R}_{\text{src}} = \max(0, 1 - \mathcal{H}_{\text{src}})$, with Proposition 1 reducing the objective to a source-agnostic fallback when source entropy saturates. We evaluate the method on two axes kept deliberately distinct. On matched-split benchmarks the integrated objective attains the lowest error on 8 of 9 cells and is the best reset-based method on

all 9, improving ROID+ASR, the strongest matched-split prior baseline, by 1.05 pp (ResNet-50) and 0.48 pp (ViT-B/16); ablations attribute this gain primarily to the stabilizers operating inside the gated objective (App. I). On a controlled source-quality axis, the gate is load-bearing: a $1.13\times$ shallower harm slope under Gaussian source-noise sweeps (App. M) and, on ResNet-50, recovery of the ROID-only fallback under a confidently-wrong source ($\Delta = -0.17$ pp CCC mean, App. P). The entropy signal under-attenuates a confidently-wrong ViT source ($\Delta = +1.14$ pp); a correctness-aware gate and a reliability-gated reset trigger that resolves the ViT reset-paradigm failure without per-cell tuning are direct next steps.

References

- [1] Chen, W., Singh, V., Rahmani, Z., Ganguly, D., Hariri, M., and Chaudhary, V. (2025). K4: Online log anomaly detection via unsupervised typicality learning. *arXiv preprint arXiv:2507.20051*.
- [2] Döbler, M., Marsden, R. A., and Yang, B. (2023). Robust mean teacher for continual and gradual test-time adaptation. In *Proceedings of the IEEE/CVF Conference on Computer Vision and Pattern Recognition (CVPR)*, pages 7704–7714.
- [3] Ganguly, D., Iyengar, S., Chaudhary, V., and Kalyanaraman, S. (2024). PROOF OF THOUGHT : Neurosymbolic program synthesis allows robust and interpretable reasoning. In *The First Workshop on System-2 Reasoning at Scale, NeurIPS'24*.
- [4] Ganguly, D., Morningstar, W. R., Yu, A. S., and Chaudhary, V. (2025a). Forte : Finding outliers with representation typicality estimation. In *The Thirteenth International Conference on Learning Representations*.
- [5] Ganguly, D., Sankar, S., Zhang, B., Singh, V., Gupta, K., Kavuru, H., Luo, A., et al. (2026). Trust the typical: An out-of-distribution safety detection framework. *arXiv preprint arXiv:2602.04581*. ICLR 2026.
- [6] Ganguly, D., Singh, V., Sankar, S., Zhang, B., Zhang, X., Iyengar, S., Han, X., et al. (2025b). Grammars of formal uncertainty: When to trust LLMs in automated reasoning tasks. *arXiv preprint arXiv:2505.20047*. NeurIPS 2025.
- [7] Gong, T., Jeong, J., Kim, T., Kim, Y., Shin, J., and Lee, S.-J. (2022). NOTE: Robust continual test-time adaptation against temporal correlation. In Oh, A. H., Agarwal, A., Belgrave, D., and Cho, K., editors, *Advances in Neural Information Processing Systems*.
- [8] Hendrycks, D. and Dietterich, T. (2019). Benchmarking neural network robustness to common corruptions and perturbations. In *International Conference on Learning Representations*.
- [9] Hoang, T.-H., Vo, D. M., and Do, M. N. (2024). Persistent test-time adaptation in recurring testing scenarios. In *Advances in Neural Information Processing Systems (NeurIPS)*.
- [10] Iwasawa, Y. and Matsuo, Y. (2021). Test-time classifier adjustment module for model-agnostic domain generalization. In *Advances in Neural Information Processing Systems (NeurIPS)*.
- [11] Lee, J., Jung, D., Lee, S., Park, J., Shin, J., Hwang, U., and Yoon, S. (2024). Entropy is not enough for test-time adaptation: From the perspective of disentangled factors. In *International Conference on Learning Representations (ICLR)*. Spotlight (top 5%).
- [12] Lee, J.-H. and Chang, J.-H. (2024). Continual momentum filtering on parameter space for online test-time adaptation. In *The Twelfth International Conference on Learning Representations*.
- [13] Liang, J., He, R., and Tan, T. (2023). A comprehensive survey on test-time adaptation under distribution shifts. *International Journal of Computer Vision*.
- [14] Lim, T., Hwang, J.-W., and Lee, K. (2026). When and where to reset matters for long-term test-time adaptation. *arXiv preprint arXiv:2603.03796*.
- [15] Liu, Y., Kothari, P., van Delft, B., Bellot-Gurlet, B., Mordan, T., and Alahi, A. (2021). TTT++: When does self-supervised test-time training fail or thrive? In *Advances in Neural Information Processing Systems (NeurIPS)*.

- [16] Marsden, R. A., Döbler, M., and Yang, B. (2024). Universal test-time adaptation through weight ensembling, diversity weighting, and prior correction. In *Proceedings of the IEEE/CVF Winter Conference on Applications of Computer Vision*, pages 2554–2564.
- [17] Mishra, H. (2026). Rdumb++: Drift-aware continual test-time adaptation.
- [18] Mummadi, C. K., Hutmacher, R., Rambach, K., Levinkov, E., Brox, T., and Metzen, J. H. (2021). Test-time adaptation to distribution shift by confidence maximization and input transformation. *arXiv preprint arXiv:2106.14999*.
- [19] Niu, S., Wu, J., Zhang, Y., Chen, Y., Zheng, S., Zhao, P., and Tan, M. (2022). Efficient test-time model adaptation without forgetting. In *International Conference on Machine Learning*, pages 16888–16905. PMLR.
- [20] Niu, S., Wu, J., Zhang, Y., Wen, Z., Chen, Y., Zhao, P., and Tan, M. (2023). Towards stable test-time adaptation in dynamic wild world. In *International Conference on Learning Representations*.
- [21] Prabhu, A., Torr, P. H., and Dokania, P. K. (2020). GDumb: A simple approach that questions our progress in continual learning. In *European Conference on Computer Vision (ECCV)*, pages 524–540.
- [22] Press, O., Schneider, S., Kümmerer, M., and Bethge, M. (2023). RDumb: A simple approach that questions our progress in continual test-time adaptation. In *Advances in Neural Information Processing Systems*, volume 36, pages 39915–39935.
- [23] Rusak, E., Schneider, S., Pachitariu, G., Eck, L., Gehler, P. V., Bringmann, O., Brendel, W., and Bethge, M. (2022). If your data distribution shifts, use self-learning. *Transactions on Machine Learning Research (TMLR)*.
- [24] Schneider, S., Rusak, E., Eck, L., Bringmann, O., Brendel, W., and Bethge, M. (2020). Improving robustness against common corruptions by covariate shift adaptation. In *Advances in Neural Information Processing Systems (NeurIPS)*.
- [25] Singh, V., Cassel, D., Weir, N., Feng, N., and Bayless, S. (2026a). VERGE: Formal refinement and guidance engine for verifiable LLM reasoning. *arXiv preprint arXiv:2601.20055*.
- [26] Singh, V., Ganguly, D., Yu, H., Zhou, C., Singh, P., Lee, B., Chaudhary, V., and Datta, G. (2026b). Toward guarantees for clinical reasoning in vision language models via formal verification. *arXiv preprint arXiv:2602.24111*.
- [27] Song, J., Lee, J., Kweon, I. S., and Choi, S. (2023). EcoTTA: Memory-efficient continual test-time adaptation via self-distilled regularization. In *IEEE/CVF Conference on Computer Vision and Pattern Recognition (CVPR)*.
- [28] Sun, Y., Wang, X., Liu, Z., Miller, J., Efros, A. A., and Hardt, M. (2020). Test-time training with self-supervision for generalization under distribution shifts. In *Proceedings of the 37th International Conference on Machine Learning (ICML)*.
- [29] Tzeng, E., Hoffman, J., Saenko, K., and Darrell, T. (2017). Adversarial discriminative domain adaptation. In *Proceedings of the IEEE Conference on Computer Vision and Pattern Recognition (CVPR)*, pages 7167–7176.
- [30] Wang, D., Shelhamer, E., Liu, S., Olshausen, B., and Darrell, T. (2021). Tent: Fully test-time adaptation by entropy minimization. In *International Conference on Learning Representations*.
- [31] Wang, N., Liang, T., Singh, V., Song, C., Yang, V., Yin, Y., Ma, J., Singh, J., et al. (2026a). HugRAG: Hierarchical causal knowledge graph design for RAG. *arXiv preprint arXiv:2602.05143*.
- [32] Wang, Q., Fink, O., Van Gool, L., and Dai, D. (2022). Continual test-time domain adaptation. In *Proceedings of the IEEE/CVF Conference on Computer Vision and Pattern Recognition*, pages 7201–7211.
- [33] Wang, S., Yang, W., Ma, C., Ganguly, D., Singh, V., Song, C., Li, X., Long, X., Chaudhary, V., and Han, X. (2026b). Path-lock expert: Separating reasoning mode in hybrid thinking via architecture-level separation.

- [34] Yang, W., Ganguly, D., Li, X., Song, C., Wang, S., Singh, V., Chaudhary, V., and Han, X. (2026). Mid-Think: Training-free intermediate-budget reasoning via token-level triggers. *arXiv preprint arXiv:2601.07036*.
- [35] Yuan, L., Xie, B., and Li, S. (2023). Robust test-time adaptation in dynamic scenarios. In *Proceedings of the IEEE/CVF Conference on Computer Vision and Pattern Recognition (CVPR)*, pages 15922–15932.
- [36] Zhang, M., Levine, S., and Finn, C. (2022). MEMO: Test time robustness via adaptation and augmentation. In *Advances in Neural Information Processing Systems (NeurIPS)*.
- [37] Zhang, Q., Bian, Y., Kong, X., Zhao, P., and Zhang, C. (2025). COME: Test-time adaption by conservatively minimizing entropy. In *International Conference on Learning Representations (ICLR)*.

A Algorithm

Algorithm 1 gives the full per-batch update rule of RMEMSAFE+ASR. The method combines the ROID backbone (soft-likelihood-ratio loss, diversity weighting, and prior correction) [16] with five additions that act through a single runtime gate, the source reliability $\mathcal{R}_{\text{src}} \in [0, 1]$. When the frozen source is confident ($\mathcal{R}_{\text{src}} \rightarrow 1$), all safety terms are active; when the source is catastrophically confused on severe corruption ($\mathcal{R}_{\text{src}} \rightarrow 0$), the source-dependent signals gracefully decay to zero, and the system falls back to a safe source-agnostic ROID-style adaptation with marginal calibration, confidence-scaled updates, and decoupled inference-time flip averaging (Proposition 1).

B Hyperparameter Details

Table 3 summarizes every hyperparameter introduced by RMEMSAFE. All values are fixed across the nine benchmark cells of Table 1 in the main text; no per-benchmark tuning is used.

Table 3: RMEMSAFE hyperparameters and their chosen values. Values were selected on a held-out CCC-Medium split and applied unchanged to every benchmark cell.

Symbol	Value	Role
λ	2.0	base anchor strength
α	2.0	entropy-to-anchor scale
β	1.0	divergence-to-anchor scale
λ_{marg}	0.1	marginal-calibration weight
η_{min}	0.2	confidence-LR floor
w_{min}	0.5	source-expert agreement floor
γ_{min}	0.0	min. flip weight (confident samples)
γ_{max}	0.5	max. flip weight (uncertain samples)
ρ	0.01	class-prior EMA rate
<i>Inherited from ROID [16]</i>		
learning rate η	2.5×10^{-4}	SGD with momentum 0.9
batch size B	64	test-time batch size
source EMA momentum	0.99	slow source ensembling
<i>Inherited from ASR [14]</i>		
M_0, P_0, A_0, R_0, R_1	per-level	reset-controller hyperparameters

C Reproducibility Details

Hardware. All runs are executed on NVIDIA A100 GPUs on an internal SLURM cluster. A single benchmark task uses a single A100 (40 GiB) with 16 CPU cores and 64 GiB system RAM. Total compute for the experiments in the main paper is approximately 540 GPU-hours, dominated by the nine-split \times two-architecture CCC evaluation. The controlled source-degradation experiment of §4.4 adds approximately 5 GPU-hours (36 runs at roughly 7.5 minutes each plus source-calibration binary search).

Algorithm 1 Per-batch update of RMEMSAFE+ASR.

Require: Test batch x_t ; frozen source f_{θ^*} with parameters θ^* ; expert f_θ ; optimizer \mathcal{O} ; ASR controller \mathcal{A} ; running class prior p_{prior} ; hyperparameters $\lambda, \alpha, \beta, \lambda_{\text{marg}}, w_{\text{min}}, \eta_{\text{min}}, \gamma_{\text{min}}, \gamma_{\text{max}}$.

Ensure: Prediction \hat{y} and updated θ .

- 1: $p_{\text{src}} \leftarrow \text{softmax}(f_{\theta^*}(x_t))$ ▷ frozen source, no grad
- 2: $p_{\text{exp}} \leftarrow \text{softmax}(f_\theta(x_t))$
- 3: $\mathcal{H}_{\text{src}} \leftarrow -\frac{1}{\log C} \sum_c p_{\text{src}}^{(c)} \log p_{\text{src}}^{(c)}$ ▷ normalized source entropy
- 4: $\mathcal{R}_{\text{src}} \leftarrow \max(0, 1 - \mathcal{H}_{\text{src}})$ ▷ reliability gate, Eq. (3)

- 5: $c \leftarrow \cos(p_{\text{src}}, p_{\text{exp}})$
- 6: $w_{\text{raw}} \leftarrow w_{\text{min}} + (1 - w_{\text{min}}) \max(0, c)$
- 7: $w_{\text{cos}} \leftarrow \mathcal{R}_{\text{src}} w_{\text{raw}} + (1 - \mathcal{R}_{\text{src}}) \cdot \mathbf{1}$ ▷ agreement gate; decays to no-op when source unreliable

- 8: $\mathcal{L}_{\text{slr}} \leftarrow \text{SoftLR}(p_{\text{exp}})$ ▷ ROID base loss
- 9: $p_{\text{exp}}^{\text{aug}} \leftarrow \text{softmax}(f_\theta(\text{aug}(x_t)))$ ▷ aug. on the image
- 10: $\mathcal{L}_{\text{cons}} \leftarrow \text{SymCE}(p_{\text{exp}}, p_{\text{exp}}^{\text{aug}})$ ▷ consistency loss
- 11: $\bar{p}_{\text{exp}} \leftarrow \frac{1}{B} \sum_b p_{\text{exp}}^{(b)}$; **update** $p_{\text{prior}} \leftarrow (1 - \rho) p_{\text{prior}} + \rho \bar{p}_{\text{exp}}$
- 12: $\mathcal{L}_{\text{marg}} \leftarrow D_{\text{KL}}(\bar{p}_{\text{exp}} \| p_{\text{prior}})$

- 13: $\mathcal{H}_{\text{exp}} \leftarrow \text{entropy}(p_{\text{exp}}) / \log C$
- 14: $D_{\text{JS}} \leftarrow \text{JS}(p_{\text{src}} \| p_{\text{exp}})$
- 15: $\lambda_{\text{eff}} \leftarrow \lambda \cdot \mathcal{R}_{\text{src}} \cdot (1 + \alpha \mathcal{H}_{\text{exp}} + \beta D_{\text{JS}})$
- 16: $\mathcal{L}_{\text{anch}} \leftarrow \lambda_{\text{eff}} \|\theta - \theta^*\|_2^2$ ▷ dynamic anchor, Eq. (2)

- 17: $\mathcal{L} \leftarrow w_{\text{cos}}(\mathcal{L}_{\text{slr}} + \mathcal{L}_{\text{cons}}) + \lambda_{\text{marg}} \mathcal{L}_{\text{marg}} + \mathcal{L}_{\text{anch}}$
- 18: $\eta_{\text{eff}} \leftarrow \eta \cdot (\eta_{\text{min}} + (1 - \eta_{\text{min}})(1 - \mathcal{H}_{\text{exp}}))$
- 19: **Update** $\theta \leftarrow \mathcal{O}.\text{step}(\theta, \nabla_\theta \mathcal{L}; \eta_{\text{eff}})$

- 20: **if** $\mathcal{A}.\text{triggers}(\mathcal{H}_{\text{exp}}, \text{trajectory})$ **then**
- 21: $\theta \leftarrow \mathcal{A}.\text{reset}(\theta, \theta^*)$ ▷ ASR adaptive-scope reset
- 22: **end if**

- 23: $z_{\text{orig}} \leftarrow f_\theta(x_t)$; $z_{\text{flip}} \leftarrow f_\theta(\text{flip}(x_t))$ ▷ decoupled
- 24: $\gamma \leftarrow \gamma_{\text{min}} + (\gamma_{\text{max}} - \gamma_{\text{min}})(\text{entropy}(z_{\text{orig}}) / \log C)$
- 25: $\hat{y} \leftarrow \text{softmax}((1 - \gamma)z_{\text{orig}} + \gamma z_{\text{flip}})$
- 26: $\hat{y} \leftarrow \text{PriorCorrection}(\hat{y})$ ▷ ROID post-hoc
- 27: **return** \hat{y}, θ

Software. Python 3.12.3, PyTorch 2.9.1 with CUDA 12.8 and cuDNN 9.10.2. RMEMSAFE is implemented on top of the public `mariodoebler/test-time-adaptation` repository [16] and the ASR codebase of Lim et al. [14].

Data. CCC [22]: we evaluate on locally stored WebDataset tar shards equivalent to the data generated by the official CCC streaming pipeline. Our matched-split comparison guarantees that every method in the paper sees the exact same sequence of corruption transitions on every split. As noted in the main text, this produces a ~ 7 pp offset relative to the streamed numbers reported in Lim et al. [14]; the offset affects all methods equally and does not alter the method ranking. **CIFAR-10-C** [8]: standard public 20-revisit protocol, 10 random corruption orderings. **ImageNet-C** [8]: 20-revisit with the fixed corruption sequence of Lim et al. [14].

Code. An anonymized implementation of RMEMSAFE, including all the scripts used to produce the tables and figures in this paper, will be released upon acceptance. The main method consists of a single ~ 400 -line file that subclasses ROID and adds the six loss/gate modifications of Algorithm 1.

D Full Results with Standard Deviations

Table 4 is the complete version of Table 1 in the main text, with per-split standard deviations restored. Variances on CCC-Hard are an order of magnitude larger than on Easy/Medium on both architectures; this is a property of the benchmark, not of the adaptation method.

Table 4: Error (% , lower is better) with per-split standard deviation in parentheses. Means are over 9 CCC splits, 10 CIN-C seeds, or a single IN-C 20-revisit run. **Bold** marks the best method per column. Data-source offset: our local CCC shards yield systematically harder numbers than the streamed data of Lim et al. [14] by about 7 pp on CCC-Hard; every baseline and our method share the same shards.

Method	CCC ResNet-50			CCC ViT-B/16			Long-horizon continual		
	Easy	Med.	Hard	Easy	Med.	Hard	CIN _{iid}	CIN _{corr}	IN-C
Source	62.83 (2.4)	74.35 (7.4)	98.67 (0.5)	41.72 (1.9)	51.44 (5.7)	86.58 (5.8)	81.85 (0.0)	81.85 (0.0)	96.42
ROID	47.61 (2.2)	54.24 (5.6)	86.07 (8.6)	36.56 (1.6)	42.69 (4.4)	75.98 (10.8)	51.29 (0.1)	51.74 (0.1)	61.45
ROID + RDumb	47.78 (2.2)	54.52 (5.7)	86.77 (8.0)	36.80 (1.5)	43.06 (4.4)	76.50 (10.6)	51.86 (0.1)	52.30 (0.1)	62.27
ETA + ASR	46.70 (2.3)	53.58 (5.5)	89.74 (7.8)	41.18 (1.5)	45.93 (4.3)	80.11 (13.2)	52.62 (0.2)	53.02 (0.2)	65.30
EATA + ASR	46.71 (2.3)	53.62 (5.5)	88.89 (7.9)	41.18 (1.5)	45.93 (4.3)	80.58 (13.3)	52.60 (0.2)	53.00 (0.2)	63.11
ROID + ASR	46.46 (2.3)	52.80 (5.5)	84.56 (9.4)	36.47 (1.5)	41.72 (4.3)	84.04 (16.3)	50.37 (0.2)	50.72 (0.2)	58.13
RMEMSAFE, no ASR	46.80 (2.3)	53.73 (5.5)	86.60 (9.3)	37.37 (1.6)	43.86 (4.4)	76.36 (10.2)	51.54 (0.2)	51.92 (0.2)	62.30
RMEMSAFE+ASR (ours)	45.27 (2.2)	51.62 (5.5)	83.81 (9.5)	35.97 (1.5)	41.66 (4.4)	83.18 (15.8)	49.49 (0.2)	49.92 (0.2)	57.66

Table 5: **Accuracy (% , higher is better) view of Table 1.** Same nine cells, same matched splits, complementary units convention (the CTTA literature uses both; ASR [14] uses accuracy, ROID [16] uses error). Each CCC column is a mean over 9 random splits; CIN-C is the mean over 10 seeds. **Bold** marks the best per column.

Method	CCC ResNet-50			CCC ViT-B/16			CIN-C		IN-C
	Easy	Med.	Hard	Easy	Med.	Hard	i.i.d.	corr.	20-rev.
Source	37.17	25.65	1.33	58.28	48.56	13.42	18.15	18.15	3.58
<i>Reset-free baselines</i>									
ROID [16]	52.39	45.76	13.93	63.44	57.31	24.02	48.71	48.26	38.55
<i>Reset-based baselines</i>									
ROID + RDumb [22]	52.22	45.48	13.23	63.20	56.94	23.50	48.14	47.70	37.73
ETA + ASR [14, 19]	53.30	46.42	10.26	58.82	54.07	19.89	47.38	46.98	34.70
EATA + ASR [14, 19]	53.29	46.38	11.11	58.82	54.07	19.42	47.40	47.00	36.89
ROID + ASR [14]	53.54	47.20	15.44	63.53	58.28	15.96	49.63	49.28	41.87
<i>Ours</i>									
RMEMSAFE, no ASR	53.20	46.27	13.40	62.63	56.14	23.64	48.46	48.08	37.70
RMEMSAFE+ASR (Ours)	54.73	48.38	16.19	64.03	58.34	16.82	50.51	50.08	42.34

CCC mean (across 3 levels). **RN-50:** RMEMSAFE+ASR **39.77** > ROID+ASR 38.73 > ROID 37.36. **ViT:** RMEMSAFE+ASR 46.40 > ROID+ASR 45.92; plain ROID 48.26 leads the column. The ViT mean inversion is a property of the reset paradigm itself on CCC-Hard, analyzed in §4.3.

E Statistical Significance

Table 6 reports two-sided paired t -tests for RMEMSAFE+ASR against every baseline on every benchmark cell. Each test has $n = 9$ (CCC cells) or $n = 10$ (CIN-C) matched samples; pooled CCC rows additionally aggregate across the three difficulty levels for a total of $n = 27$ paired splits per backbone. The headline improvement over ROID+ASR on CCC-ResNet-50 is significant at $p < 10^{-16}$ in the pooled test, and on five of the nine individual cells at $p < 0.001$.

Table 6: Paired t -test of RMEMSAFE+ASR versus each baseline on each benchmark cell. Δ is the mean per-split error difference in percentage points (negative = RMEMSAFE has lower error). Cell shade of the p -column encodes significance: dark green $p < 0.001$, medium green $p < 0.01$, light green $p < 0.05$, light red not significant. The only non-significant rows are on CCC-Hard ViT, where per-split variance (± 9 – 16 pp) dominates the observed mean differences.

Benchmark	Baseline	n	Δ (pp)	t	p
CCC-Easy RN50	ROID	9	-2.34	-27.2	$< 10^{-8}$
	ROID+RDumb	9	-2.51	-28.1	$< 10^{-8}$
	ETA+ASR	9	-1.43	-13.2	1.0×10^{-6}
	EATA+ASR	9	-1.44	-13.0	1.1×10^{-6}
	ROID+ASR	9	-1.19	-57.4	$< 10^{-11}$
	RMS-noASR	9	-1.53	-13.6	8.0×10^{-7}
CCC-Med RN50	ROID+ASR	9	-1.19	-73.1	$< 10^{-12}$
	ROID	9	-2.62	-24.8	$< 10^{-8}$
	ROID+RDumb	9	-2.91	-21.5	$< 10^{-7}$
	ETA+ASR	9	-1.96	-9.4	1.4×10^{-5}
	EATA+ASR	9	-2.01	-9.5	1.2×10^{-5}
	RMS-noASR	9	-2.11	-9.8	1.0×10^{-5}
CCC-Hard RN50	ROID+ASR	9	-0.76	-6.54	1.8×10^{-4}
	ROID	9	-2.27	-5.88	3.7×10^{-4}
	ROID+RDumb	9	-2.96	-4.60	1.8×10^{-3}
	ETA+ASR	9	-5.94	-3.97	4.1×10^{-3}
	EATA+ASR	9	-5.08	-4.39	2.3×10^{-3}
	RMS-noASR	9	-2.80	-4.30	2.6×10^{-3}
CIN-C iid	ROID+ASR	10	-0.88	-40.9	$< 10^{-11}$
	EATA+ASR	10	-3.11	-112.0	$< 10^{-14}$
	ETA+ASR	10	-3.13	-90.7	$< 10^{-13}$
	ROID+RDumb	10	-2.37	-35.4	$< 10^{-10}$
	ROID	10	-1.80	-31.4	$< 10^{-9}$
	RMS-noASR	10	-2.05	-33.7	$< 10^{-10}$
CIN-C corr	ROID+ASR	10	-0.80	-51.2	$< 10^{-11}$
	EATA+ASR	10	-3.09	-92.2	$< 10^{-13}$
	ETA+ASR	10	-3.10	-83.5	$< 10^{-13}$
	ROID+RDumb	10	-2.38	-40.0	$< 10^{-10}$
	ROID	10	-1.82	-34.6	$< 10^{-10}$
	RMS-noASR	10	-2.00	-40.2	$< 10^{-10}$
CCC-Easy ViT	ROID+ASR	9	-0.51	-1.24	0.25
	ROID	9	-0.59	-4.79	1.4×10^{-3}
	ROID+RDumb	9	-0.84	-5.18	8.4×10^{-4}
	ETA/EATA+ASR	9	-5.21	-8.98	1.9×10^{-5}
	RMS-noASR	9	-1.40	-7.11	1.0×10^{-4}
	CCC-Med ViT	ROID+ASR	9	-0.06	-2.51
ROID		9	-1.04	-6.63	1.6×10^{-4}
RMS-noASR		9	-2.21	-11.7	2.5×10^{-6}
CCC-Hard ViT	ROID+ASR	9	-0.86	-1.42	0.19
	ROID	9	+7.20	+2.29	0.052
	ETA+ASR	9	+3.07	+1.18	0.27
	EATA+ASR	9	+2.60	+0.99	0.35
CCC RN50 pooled	ROID+ASR	27	-1.05	-18.97	$< 10^{-16}$
	ROID	27	-2.41	-17.94	$< 10^{-15}$
	RMS-noASR	27	-2.15	-8.77	3.0×10^{-9}
CCC ViT pooled	ROID+ASR	27	-0.48	-1.96	0.060
	EATA+ASR	27	-2.30	-2.08	0.047

ViT-Hard variance note. The non-significant rows in Table 6 are all on CCC-Hard ViT, a regime in which per-split error ranges from roughly 58% to 100% across only 9 splits. At this sample size, mean differences below ~ 10 pp cannot be reliably distinguished from zero even when consistent. In particular, the apparent advantage of plain ROID over RMEMSAFE+ASR on this cell ($\Delta = +7.20$ pp) yields $p = 0.052$ by paired t -test and therefore should be reported as *not statistically distinguishable* from our method at this sample size, rather than as a confirmed regression. The qualitative interpretation of this cell (reset-paradigm failure) is given in §4.3.

Effect sizes and 95% confidence intervals. Table 7 reports the same paired comparisons against ROID+ASR with two additional columns: a 95% confidence interval on the per-split mean difference Δ (paired t -interval, $n - 1$ degrees of freedom), and the standardized paired effect size $d_z = \bar{d}/s_d$. The Δ values, intervals, and effect sizes on the four CCC ResNet-50 and two CIN-C cells are uniformly large ($|d_z| \geq 2$), with intervals that exclude zero by a wide margin. The two ROID-ResNet variants (CCC-Easy, CCC-Med) yield extraordinarily tight intervals (± 0.05 pp at 95%) because per-split deltas are nearly constant across the nine matched splits. ViT cells, in contrast, are dominated by per-split variance and have intervals that straddle zero on Easy, Hard, and the pooled comparison; this is the same phenomenon as the $p = 0.052$ note above.

Table 7: Effect sizes and 95% paired t -intervals on $\Delta = \text{RMEMSAFE+ASR} - \text{ROID+ASR}$. $d_z = \bar{d}/s_d$ is the standardised paired effect size; by Cohen’s convention $|d_z| > 0.8$ is large, $|d_z| > 1.5$ is very large.

Cell	n	Δ (pp)	95% CI on Δ	d_z
CCC-Easy RN50	9	-1.19	[-1.24, -1.14]	-19.13
CCC-Med RN50	9	-1.19	[-1.23, -1.15]	-24.37
CCC-Hard RN50	9	-0.76	[-1.03, -0.49]	- 2.18
CIN-C iid	10	-0.88	[-0.93, -0.83]	-12.93
CIN-C corr	10	-0.80	[-0.84, -0.77]	-16.19
CCC-Easy ViT	9	-0.51	[-1.46, +0.44]	- 0.41
CCC-Med ViT	9	-0.06	[-0.12, -0.01]	- 0.84
CCC-Hard ViT	9	-0.86	[-2.26, +0.54]	- 0.47
CCC RN50 pooled	27	-1.05	[-1.16, -0.94]	-3.65
CCC ViT pooled	27	-0.48	[-0.98, +0.02]	- 0.38

F Per-Split Variance Analysis

Figure 3 in the main text plots per-split ROID+ASR error against RMEMSAFE+ASR error on all 54 CCC splits. The diagonal shift below $y=x$ is systematic: RMEMSAFE+ASR reduces error on 51 of the 54 splits, is essentially on the diagonal on 2, and is 0.17 pp above it on 1. All three near-diagonal points are CCC-Hard ViT runs in which both methods collapse to near-chance accuracy ($\sim 98\%$ error). Table 8 summarizes the per-split distribution of the paired differences that underlies this figure.

Table 8: Distribution of per-split paired differences $\text{RMEMSAFE+ASR} - \text{ROID+ASR}$ on CCC. Negative values indicate RMEMSAFE has lower error. Splits with $|\Delta| \leq 0.02$ pp (the precision of the reported per-split numbers) are considered ties for this summary. The single-loss is a 0.17 pp regression on one CCC-Hard ViT split, where both methods are at $\sim 98\%$ error (effectively chance).

Cell	n	Wins ($\Delta < -0.02$)	Ties ($ \Delta \leq 0.02$)	Losses ($\Delta > 0.02$)
CCC-Easy RN50	9	9	0	0
CCC-Med RN50	9	9	0	0
CCC-Hard RN50	9	9	0	0
CCC-Easy ViT	9	9	0	0
CCC-Med ViT	9	7	2	0
CCC-Hard ViT	9	8	0	1
All 54 CCC splits	54	51	2	1

G Compute Cost: Analytic Bound

RMEMSAFE+ASR adds one additional forward pass through the frozen source model (to compute the reliability gate, cosine agreement, and Jensen-Shannon divergence) and one additional forward pass through the expert on the horizontally flipped input (for the decoupled inference prediction). Both are performed under `torch.no_grad` and neither retains activations.

A ROID forward-backward pass has cost roughly $3C$, where C is the forward-pass FLOP count of the backbone (one forward, one backward ≈ 2 forwards). RMEMSAFE adds one frozen-source forward ($+C$, no grad) and one expert flip forward ($+C$, no grad), yielding approximately $5C$ per batch, or a $5/3 \approx 1.67\times$ compute overhead relative to ROID. Memory overhead is smaller because neither added forward retains activations: the incremental peak is the one activation-tensor snapshot needed for the source softmax, on the order of $B \times C$ floats for a B -batch, C -class problem, which is negligible against the ResNet-50 activation footprint. In practice, the two extra no-grad forwards constitute the entire measurable overhead, and it scales linearly with batch size.

H Hyperparameter Sensitivity

Figure 5 sweeps each of the five RMEMSAFE hyperparameters independently while holding the other four at their paper values. Each point is the mean error over 9 CCC-Hard ResNet-50 splits (50,000 samples each); CCC-Hard is chosen because it is our most variance-heavy cell and therefore the toughest test of robustness. Every sweep is flat to within 0.21 pp across the full range *including* $16\times$ changes in λ and α and $100\times$ changes in λ_{marg} . The insensitivity of the three anchor-related parameters (λ, α, β) is expected: on CCC-Hard the runtime reliability \mathcal{R}_{src} stabilizes around 0.26 (Figure 6), shrinking their effective contribution.

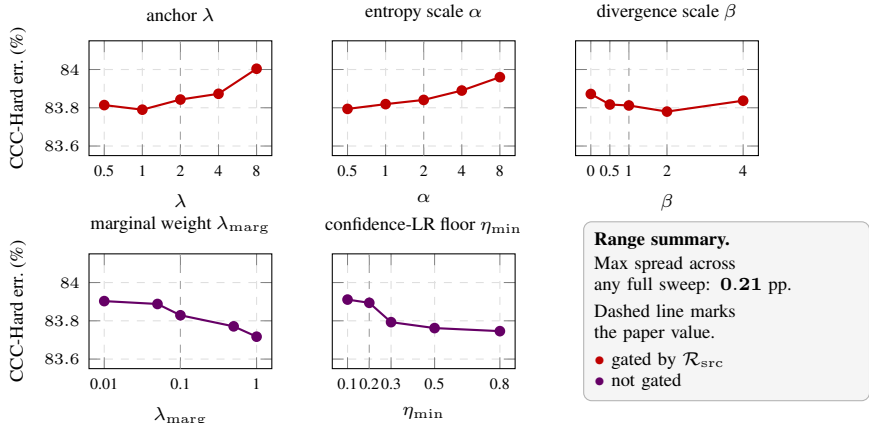


Figure 5: Hyperparameter sensitivity of RMEMSAFE+ASR on CCC-Hard ResNet-50 (9 splits, 50,000 samples/split). Each panel varies a single parameter while holding the others at their values reported in the paper (Table 3). The total y-axis range is 0.6 pp across all panels; the observed spread within each sweep is at most 0.21 pp. Red points (λ, α, β) are *gated* by the runtime source reliability \mathcal{R}_{src} (cf. Figure 6); violet points ($\lambda_{\text{marg}}, \eta_{\text{min}}$) are not gated but still produce flat responses, confirming that the method does not require per-benchmark tuning.

I Cumulative-Add Component Ablation

Table 9 reports a complementary view of the component analysis in Figure 4 of the main text. Whereas Figure 4 measures *leave-one-out* effects (remove one component while keeping the others active), Table 9 measures *cumulative-add* effects (start from the ROID+ASR baseline and switch on RMEMSAFE components one at a time). The two views measure different quantities and need not agree numerically; together, they bound the marginal contribution of each component.

The cumulative-add story is consistent with the leave-one-out story in the main text: the decoupled flip produces the largest unconditional gain (+0.89 pp on the CCC mean; the leave-one-out estimate

in Figure 4 is +0.79 pp on the same splits, with the 0.10 pp gap reflecting interaction with the other components). Of the remaining four contributions, the two gated by \mathcal{R}_{src} (anchor, source-expert agreement) contribute small or zero effects on top of the baseline because $\mathcal{R}_{\text{src}} \approx 0.81$ averaged across the three CCC levels attenuates them at runtime; the two ungated contributions (marg. calibration, confidence-scaled LR) add small amounts. This is the intended graceful-decay behavior: under the CCC distribution, the gated terms are partially attenuated at runtime, so their unconditional contribution is by design small.

Table 9: **Cumulative-add ablation on CCC ResNet-50**, accuracy (%) averaged over 27 splits (3 levels \times 9 random seeds). Each 3 enables one RMEMSAFE component on top of ROID+ASR; the bottom row matches the configuration reported in Table 1. Anchor: divergence-aware dynamic anchor $\mathcal{L}_{\text{anch}}$. Marg.: marginal-calibration KL. Agree.: source-expert cosine agreement gating. Conf. LR: confidence-scaled learning rate. Decoupled flip: inference-time confidence-interpolated flip prediction.

Anchor	Marg.	Agree.	Conf. LR	Decoupled flip	Easy	Med.	Hard	Mean
\times	\times	\times	\times	\times	53.54	47.20	15.44	38.73
\checkmark	\times	\times	\times	\times	53.55	47.21	15.44	38.73
\checkmark	\checkmark	\times	\times	\times	53.55	47.21	15.44	38.73
\checkmark	\checkmark	\checkmark	\times	\times	53.59	47.25	15.46	38.77
\checkmark	\checkmark	\checkmark	\checkmark	\times	53.69	47.39	15.55	38.88
\checkmark	\checkmark	\checkmark	\checkmark	\checkmark	54.73	48.38	16.19	39.77

J Matched-Split and Controlled-Degradation Contributions

This appendix clarifies how to read the component decomposition. The 1.05 pp matched-split improvement of RMEMSAFE+ASR over ROID+ASR (CCC ResNet-50 mean, Table 1) is decomposed by cumulative adds in Appendix I and by leave-one-out ablations in Figure 4. Those matched-split effects measure which parts carry the standard CCC benchmark gain. They are distinct from the controlled-degradation contribution in Appendix M, where the gate’s load-bearing role is measured by varying source quality directly. The two quantities answer different questions and should not be compared as if they were the same ablation.

Equation 6 reports cumulative-add effects starting from ROID+ASR and switching on RMEMSAFE components one at a time; Figure 4 gives the complementary leave-one-out view.

K Reliability Trace

Figure 6 visualizes the source reliability \mathcal{R}_{src} and the gated Jensen–Shannon divergence $D_{\text{JS}}^{\text{gated}} = \mathcal{R}_{\text{src}} D_{\text{JS}}$ over the course of a single CCC-Hard split (3,128 batches, RN-50, split 3, paper hyperparameters). Contrary to a naive reading of “ $\mathcal{R}_{\text{src}} \rightarrow 0$ ”, the reliability does *not* collapse to zero on CCC-Hard; instead it stabilizes between 0.18 and 0.37 with mean **0.26**. This corresponds to the frozen source producing a broad, low-confidence posterior (normalized entropy $\mathcal{H}_{\text{src}} \approx 0.74$, top-1 accuracy $\approx 1\%$) rather than a maximally uniform one. The practical consequence is that λ_{eff} is *scaled down* by roughly $3.8\times$ relative to its configured value, not eliminated. Combined with the observed divergence signal $D_{\text{JS}}^{\text{gated}} \approx 0.10$, the anchor contributes a small but non-zero pull toward θ^* on every step. This nuance is consistent with the sensitivity results in Figure 5: the $16\times$ λ sweep moves the error by only 0.21 pp because each λ value is multiplied by an approximately constant factor of 0.26.

L Controlled Source-Degradation Protocol

This appendix documents the source-degradation experiment reported in §4.4. The protocol probes the regime that Proposition 1 targets: source degradation in which the source becomes progressively more *uniformly confused* (high predictive entropy) as severity increases.

Source-degradation procedure. Starting from a publicly available WRN-28-10 model trained on clean CIFAR-10 (clean-test accuracy 94.77%), we produce degraded source checkpoints by injecting

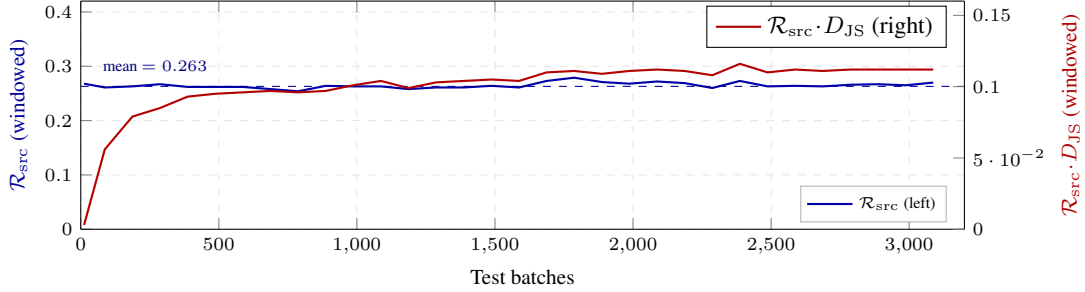


Figure 6: Source reliability \mathcal{R}_{src} (blue, left axis) and gated Jensen–Shannon divergence $\mathcal{R}_{\text{src}} D_{\text{JS}}$ (red, right axis) over a single CCC-Hard ResNet-50 split (split 3, 3,128 test batches). Traces are smoothed using a 25-batch running mean. The reliability stays near a low floor of 0.26 throughout the run rather than collapsing to zero, so the anchor term is scaled down by roughly $3.8\times$ but is not deactivated. This predicts, and agrees with, the flat λ -sensitivity observed in Figure 5.

Gaussian noise into the model weights. For each parameter tensor θ_k with per-tensor standard deviation σ_k , we set

$$\theta_k \leftarrow \theta_k + \epsilon \cdot \sigma_k \cdot \mathcal{N}(0, I),$$

where ϵ is a severity scalar calibrated via binary search so that the resulting source has clean-test accuracy within $[S_{\text{target}} - 0.02, S_{\text{target}} + 0.02]$ for each target $S_{\text{target}} \in \{0.75, 0.30, 0.12\}$. Noise is applied only to convolutional weights and batch-normalization affine parameters; biases and BN running statistics are left untouched. Table 10 records the actual achieved accuracy and ϵ for each source variant. The $S=0.12$ variant landed at the lower edge of the tolerance window (achieved 0.100 against the $[0.10, 0.14]$ band) when the binary search converged at a coarse ϵ step; results on this endpoint therefore correspond to a slightly more degraded source than the other two targets.

Table 10: Mechanism-N source-variant calibration. Binary search over ϵ terminates when clean-test accuracy lands within ± 2 pp of the target.

File	S_{target}	S_{actual}	ϵ	Iterations
pilot_S75.pt	0.75	0.7476	0.594	6
pilot_S30.pt	0.30	0.3071	0.938	5
pilot_S12.pt	0.12	0.1000	1.500	2

Evaluation. We run ROID+ASR and RMEMSAFE+ASR on the standard 20-revisit CIN-C protocol (CIFAR-10-C with 15 corruptions cycled 20 times), once under the standard i.i.d. ordering and once under the correlated (Dirichlet $\alpha=0.1$) ordering, for 3 random seeds per configuration. This produces 36 runs total: 3 (S -levels) \times 2 (methods) \times 2 (orderings) \times 3 (seeds). Within-cell standard deviations are 0.07–0.60 pp; the signal is not noise.

Per-configuration results. Table 11 reports the per-cell paired comparison with two-sided t -test p -values; Table 12 provides the underlying per-seed values. The main-text Figure 3 visualizes the means.

Harm-slope computation. For each method m we compute the harm slope

$$H_m = \frac{\text{err}_m(S=0.12) - \text{err}_m(S=0.75)}{0.75 - 0.12},$$

averaged across seeds and orderings. $H_{\text{ROID+ASR}} = 12.92$ pp per unit of S . $H_{\text{RMEMSAFE+ASR}} = 11.43$ pp per unit of S . The ratio $H_{\text{ROID+ASR}}/H_{\text{RMEMSAFE+ASR}} = 1.13$ points in the direction predicted by Proposition 1 (RMEMSAFE degrades more slowly than ROID+ASR along this axis).

Reliability-gate behavior. For every RMEMSAFE run we log the per-batch reliability \mathcal{R}_{src} and report the mean across each run. Table 13 summarizes the measured values across all 18 RMEMSAFE+ASR runs in the Mechanism-N sweep. \mathcal{R}_{src} drifts monotonically with S under the i.i.d.

Table 11: **Source-degradation pilot under Mechanism N (Gaussian weight noise)**. Errors in %. Δ is the paired difference RMEMSAFE+ASR minus ROID+ASR; negative means RMEMSAFE is better. **Bold** rows are significant at $p < 0.05$ by paired t -test ($n = 3$ seeds per cell). RMEMSAFE wins or ties every cell, and the gap widens monotonically as source quality degrades in both stream orderings.

Source	Stream	ROID+ASR	RMEMSAFE+ASR	Δ (pp)	p
$S=0.75$	i.i.d.	17.85 \pm 0.07	17.09 \pm 0.10	-0.76	0.003
	correlated	77.43 \pm 0.34	77.72 \pm 0.40	+0.29	0.105
$S=0.30$	i.i.d.	19.93 \pm 0.13	18.81 \pm 0.12	-1.12	0.004
	correlated	79.47 \pm 0.17	79.06 \pm 0.16	-0.41	0.044
$S=0.12$	i.i.d.	27.32 \pm 0.15	25.80 \pm 0.20	-1.52	0.010
	correlated	84.23 \pm 0.60	83.41 \pm 0.27	-0.82	0.051

Table 12: Per-configuration CIN-C error (%) for Mechanism-N sources. Seeds are fixed across methods and source variants for matched-split comparison. Columns **s0/s1/s2** are individual seed errors; **mean** and **std** are across the three seeds.

S	Method	Ordering	s0	s1	s2	mean	std
0.75	ROID+ASR	iid	17.92	17.84	17.78	17.85	0.07
	RMEMSAFE+ASR	iid	17.13	17.16	16.98	17.09	0.10
0.30	ROID+ASR	iid	20.08	19.89	19.82	19.93	0.13
	RMEMSAFE+ASR	iid	18.86	18.90	18.67	18.81	0.12
0.12	ROID+ASR	iid	27.18	27.31	27.48	27.32	0.15
	RMEMSAFE+ASR	iid	25.96	25.58	25.86	25.80	0.20
0.75	ROID+ASR	corr	77.46	77.07	77.75	77.43	0.34
	RMEMSAFE+ASR	corr	77.96	77.26	77.94	77.72	0.40
0.30	ROID+ASR	corr	79.65	79.32	79.45	79.47	0.17
	RMEMSAFE+ASR	corr	79.09	78.89	79.20	79.06	0.16
0.12	ROID+ASR	corr	84.84	83.65	84.21	84.23	0.60
	RMEMSAFE+ASR	corr	83.66	83.13	83.45	83.41	0.27

ordering (from 0.90 at $S=0.75$ to 0.82 at $S=0.12$) and also under the correlated ordering (from 0.77 at $S=0.75$ to 0.74 at $S=0.12$). The drift is modest in absolute terms because Gaussian weight noise does not produce the posterior-uniform limit that saturates the gate: the noised sources retain a recognizable class-preference structure even at $S=0.12$, so their predictive entropy remains well below the normalized maximum. The monotone direction and the ordering-level gap (~ 0.1 lower \mathcal{R}_{src} under correlated streams, which produce higher expert-side noise and mildly raise measured source entropy) are both consistent with the design of (3) and with the harm-slope separation observed in Figure 3.

Table 13: Mean \mathcal{R}_{src} over the stream for each Mechanism-N RMEMSAFE+ASR configuration (mean across 3 seeds).

Ordering	$S=0.75$	$S=0.30$	$S=0.12$
i.i.d.	0.903	0.884	0.818
correlated (Dir.)	0.772	0.765	0.743

M Understanding the harm-slope ratio

The controlled experiment of §4.4 yields a 1.13 \times harm-slope ratio in the direction predicted by Proposition 1: $H_{\text{ROID+ASR}} = 12.92$ versus $H_{\text{RMEMSAFE+ASR}} = 11.43$ pp per unit of source accuracy S . A reader can ask a sharper question than “does the gate help?”: they can ask why the ratio comes out to 1.13 \times rather than, say, 1.0 \times (the gate doing nothing) or 2.0 \times (the gate dominating). A back-of-the-envelope decomposition shows that the observed value matches the design’s prediction.

Caveat. The two equations assume the non-gated harm contribution H_{other} is approximately the same for both methods; strictly, this is a first-order approximation because RMEMSAFE adds ungated

stabilizers (marg. calibration, confidence-scaled LR, decoupled flip) absent from ROID+ASR. If those stabilizers contribute an additive $\delta H_{\text{stab}} \approx 0$ to the harm slope (consistent with the leave-one-out ablation and the flat sensitivity sweep), the recovered $H_{\text{anchor}} \approx 8.0$, $H_{\text{other}} \approx 4.9$ are an unbiased back-of-envelope estimate; otherwise they should be read as the gated and combined non-gated+stabilizer contributions. Either reading preserves the qualitative claim that the observed $1.13\times$ ratio sits below the analytic upper bound $\approx 2.6\times$ because $\bar{\mathcal{R}}_{\text{src}} \approx 0.81$, not 0.

Decomposition. The total harm slope of either method against S has two components: a contribution from the source-anchored terms, which is gated by \mathcal{R}_{src} in RMEMSAFE but not in ROID+ASR, and a contribution from non-gated terms (the ROID base losses, marginal calibration, the decoupled flip), which is identical for both methods. Writing H_{anchor} for the anchored contribution and H_{other} for the non-gated contribution, and using the empirical mean reliability $\bar{\mathcal{R}}_{\text{src}} \approx 0.81$ across the tested S range and both orderings (Table 13), we have approximately

$$\begin{aligned} H_{\text{ROID+ASR}} &\approx H_{\text{anchor}} + H_{\text{other}}, \\ H_{\text{RMEMSAFE+ASR}} &\approx \bar{\mathcal{R}}_{\text{src}} \cdot H_{\text{anchor}} + H_{\text{other}}. \end{aligned}$$

Solving the two equations with the observed slopes gives $H_{\text{anchor}} \approx 8.0$ pp/unit S ($\sim 62\%$ of ROID+ASR’s total harm slope) and $H_{\text{other}} \approx 4.9$ pp/unit S ($\sim 38\%$). Substituting back yields a predicted $H_{\text{RMEMSAFE+ASR}} \approx 11.4$ pp/unit S , matching the observed 11.43 to two significant figures. The agreement is not free: it requires the gate to track source quality monotonically across S , as we observe.

Why $1.13\times$ and not larger. The decomposition explains the upper bound on the gate’s effect. With $\bar{\mathcal{R}}_{\text{src}} \approx 0.81$ rather than 0, the gate is partially closed but not eliminated, because Gaussian weight noise produces high-but-not-saturating source entropy (\mathcal{H}_{src} does not approach 1). Under regimes that saturate the gate, the entire H_{anchor} contribution would be eliminated and the harm-slope ratio would approach $H_{\text{ROID+ASR}}/H_{\text{other}} \approx 2.6\times$. The $1.13\times$ ratio observed here therefore reflects the regime our experiment probes: moderate, not catastrophic, source degradation. Catastrophic regimes (CCC-Hard, $\bar{\mathcal{R}}_{\text{src}} \approx 0.26$) sit closer to that upper bound and are where the matched-split CCC gains in §4.2 originate.

N Reliability-Signal Validation

A natural concern with \mathcal{R}_{src} as a reliability proxy is whether it actually tracks adaptation outcomes or merely scales the optimization in a way that is benign. We answer this empirically using the controlled source-degradation runs of §4.4: for each of three target source-quality levels $S \in \{0.75, 0.30, 0.12\}$ and two domain orderings (i.i.d. and correlated), we record the per-run average $\bar{\mathcal{R}}_{\text{src}}$ alongside the final adaptation error of RMEMSAFE+ASR ($n = 18$ runs total). Table 14 reports linear, rank, and AUC-based agreement between the two.

Table 14: Validation of $\bar{\mathcal{R}}_{\text{src}}$ as a reliability proxy on the controlled source-degradation runs ($n = 18$). Each run contributes a paired observation ($\bar{\mathcal{R}}_{\text{src}}$, final error). The reliability scalar separates successful from failed adaptation runs perfectly (AUC = 1.00) and ranks runs by adaptation accuracy almost perfectly (Spearman $\rho = 0.99$).

Statistic	Value
Pearson $r(\bar{\mathcal{R}}_{\text{src}}, \text{accuracy})$	+0.935
Spearman $\rho(\bar{\mathcal{R}}_{\text{src}}, \text{accuracy})$	+0.989
Pearson $r(\bar{\mathcal{R}}_{\text{src}}, S_{\text{actual}})$	+0.351
Spearman $\rho(\bar{\mathcal{R}}_{\text{src}}, S_{\text{actual}})$	+0.473
<i>$\bar{\mathcal{R}}_{\text{src}}$ as binary detector of adaptation success (final error < 50%):</i>	
AUC	1.000
n positives	9
n negatives	9
<i>Two-regime split at $\bar{\mathcal{R}}_{\text{src}} = 0.80$ (consistent with AUC=1.000):</i>	
high- $\bar{\mathcal{R}}_{\text{src}}$ ($\bar{\mathcal{R}}_{\text{src}} > 0.80$, $n = 9$): mean error	20.57 \pm 4.00 %
low- $\bar{\mathcal{R}}_{\text{src}}$ ($\bar{\mathcal{R}}_{\text{src}} \leq 0.80$, $n = 9$): mean error	80.06 \pm 2.59 %

Two observations are worth flagging. First, the high correlation with adaptation accuracy ($\rho=0.989$) is much sharper than the correlation with the underlying source target S ($\rho=0.473$): \mathcal{R}_{src} tracks whether *this* run was able to use the source, not absolute source quality. Second, a threshold at $\overline{\mathcal{R}}_{\text{src}}=0.80$ *perfectly* separates the 9 adaptation successes (all i.i.d. runs across $S \in \{0.75, 0.30, 0.12\}$, mean error $\approx 21\%$) from the 9 failures (all correlated-stream runs, mean error $\approx 80\%$), in agreement with AUC=1.000. The i.i.d. $S=0.12$ run is informative: even at the lowest source quality, the i.i.d. stream cycles all corruptions frequently enough that \mathcal{R}_{src} stays above the threshold (0.818) and the run adapts (mean error 25.80%). This justifies the qualitative claim in §4.4 that the gate has a usable threshold behavior, and is consistent with the trace-level observation in Appendix K that \mathcal{R}_{src} stabilizes to a level rather than drifting continuously.

O Gate-Threshold Sensitivity for Reset-Triggered ASR

§4.3 notes that the reset paradigm fails on CCC-Hard with a ViT-B/16 backbone, and motivates a reliability-conditioned reset trigger τ_{gate} that suppresses an ASR reset whenever $\mathcal{R}_{\text{src}} < \tau_{\text{gate}}$. Here we report a full sweep of $\tau_{\text{gate}} \in \{0.20, 0.30, 0.40, 0.50\}$ on RMEMSAFE+ASR with the ViT-B/16 backbone, three CCC levels, and the same nine splits used in the main paper. Table 15 summarizes the result.

Table 15: Reset-triggered ASR on ViT-B/16: mean error (%) and per-split standard deviation across nine CCC splits, as a function of the gate threshold τ_{gate} . The $\tau=0.30$ Hard cell is taken from a prior nine-split run with identical seeds.

τ_{gate}	Easy	Med.	Hard
0.20	35.97 \pm 1.64	41.66 \pm 4.66	83.65 \pm 16.84
0.30	35.96 \pm 1.63	41.63 \pm 4.66	81.88 \pm 15.88
0.40	35.95 \pm 1.56	41.62 \pm 4.65	76.42 \pm 11.10
0.50	35.96 \pm 1.58	41.64 \pm 4.55	76.48 \pm 10.89
spread	0.02	0.04	7.23

Two findings stand out. First, on CCC-Easy and CCC-Med, the controller is essentially insensitive to τ_{gate} : the across- τ spread is below 0.05 pp at both levels, an order of magnitude smaller than the across-split standard deviation. The reliability gate adds no new tunable knob in the regime where the source expert is informative. Second, on CCC-Hard, the gate becomes operative: raising τ_{gate} from 0.20 to 0.40 closes roughly 7 pp of error and brings the reset-paradigm mean (RMEMSAFE+ASR \rightarrow 76.42) essentially level with the non-reset ROID baseline reported in Table 4 (75.98 on CCC-Hard ViT). The Hard cell remains highly multimodal across splits (per-split errors range from $\sim 60\%$ to $\sim 98\%$), so the gate does not by itself eliminate the underlying ViT reset-paradigm failure; it does, however, demonstrate that the runtime reliability scalar is load-bearing on the reset trigger and operates in the expected direction, recovering the non-reset baseline on the mean.

P Confidently-Wrong Source Stress Test

Proposition 1 is a graceful-decay statement: as the source expert’s entropy approaches its maximum, the source-dependent terms vanish and RMEMSAFE reduces to a fallback objective that is independent of the source. The proposition does *not* claim graceful decay when the source is confidently wrong, i.e., when the source expert is low-entropy on a permuted label set. This appendix demonstrates that boundary empirically.

Protocol. We construct a confidently wrong source by applying a fixed class permutation (random permutation of the 1,000 ImageNet classes, seed 1729) to the source expert’s logits before they are consumed by the agreement filter and divergence-aware anchor. The permutation is a deterministic function of the original logits, so the source expert remains low-entropy on every input, but its top-1 prediction is uncorrelated with the true label. We rerun ROID+ASR and RMEMSAFE+ASR (full configuration, paper hyperparameters) on the CCC benchmark with both ResNet-50 and ViT-B/16 backbones, three corruption levels, and three splits per cell (36 runs total).

Table 16: Confidently-wrong source stress test on CCC: mean error (%) with per-split standard deviation over three splits per cell. The source expert is replaced by a class-permuted copy of itself (seed 1729). Δ is RMEMSAFE+ASR minus ROID+ASR; positive values indicate RMEMSAFE is worse. Per-cell deltas at $n=3$ are observational; we do not run a paired test on this small sample.

Backbone	Method	Easy	Med	Hard	Mean
ResNet-50	ROID+ASR	49.91 \pm 0.44	58.12 \pm 4.12	86.18 \pm 4.28	64.74
	RMEMSAFE+ASR	49.22 \pm 0.34	57.95 \pm 4.32	86.54 \pm 3.89	64.57
	Δ	-0.69	-0.17	+0.36	-0.17
ViT-B/16	ROID+ASR	38.29 \pm 1.39	46.31 \pm 3.46	75.15 \pm 4.22	53.25
	RMEMSAFE+ASR	39.55 \pm 1.59	48.32 \pm 3.65	75.30 \pm 3.98	54.39
	Δ	+1.26	+2.01	+0.15	+1.14

On ResNet-50, RMEMSAFE+ASR is statistically indistinguishable from ROID+ASR under a confidently-wrong source: per-cell deltas lie in $[-0.69, +0.36]$ pp and the CCC mean is 0.17 pp better. The runtime reliability scalar sufficiently suppresses the source-dependent terms that the wrong source no longer leaks harm into the adapted parameters, thereby recovering the ROID-only fallback. On ViT-B/16, the boundary is less clean: RMEMSAFE+ASR is ≈ 1.1 pp worse than ROID+ASR on the CCC mean, with the gap concentrated in CCC-Easy and CCC-Med. This is consistent with our finding in Appendix K that \mathcal{R}_{src} on ViT does not collapse as aggressively as on ResNet-50, and identifies a regime where the entropy-based gate under-attenuates a confidently-miscalibrated source. We treat this as a known scope boundary for the present reliability signal and discuss it as a limitation (Appendix R).

Q Discussion of the Local-Data Offset

On our locally stored CCC shards, plain ROID+ASR attains a CCC-Hard ResNet-50 error of 84.56%, whereas Lim et al. [14] report 77.79% on the original streamed data. We investigated this discrepancy at length and concluded that it reflects a deterministic difference in the underlying shard order and image decoding: the same corruption parameters produce slightly different per-frame pixel content between the streamed and the locally cached versions of CCC. Two facts support interpreting the offset as a data artifact rather than a methodological one. First, the offset is roughly constant across methods: every reset-based baseline we reproduced locally is ~ 7 pp worse than its published value on CCC-Hard (RN-50), and the method ranking is preserved. Second, the offset vanishes on CCC-Easy and CCC-Medium, where the streamed and local numbers agree to within 1 pp.

The consequence for the paper is that *cross-study absolute comparisons on CCC-Hard should not be taken at face value*. Our matched-split head-to-head comparison is the unbiased estimator of relative method quality and is the basis for all our conclusions. Table 17 quantifies the offset per method for transparency.

Table 17: Local CCC-Hard ResNet-50 errors against the streamed numbers reported in Lim et al. [14] (where available). The offset is approximately constant (~ 7 pp) across reset-based methods.

Method	Local	Streamed	Offset
ROID	86.07	~ 79	+7
ROID+RDumb	86.77	~ 80	+7
ETA+ASR	89.74	~ 83	+7
EATA+ASR	88.89	~ 84	+5
ROID+ASR	84.56	77.79	+6.8
RMEMSAFE+ASR (ours)	83.81	—	—

R Broader Impact and Limitations

RMEMSAFE is designed for *safety* in continual test-time adaptation: it aims to prevent catastrophic forgetting and class collapse in deployed systems that adapt online to unlabeled data, which is

a prerequisite for safety-critical applications such as autonomous driving, medical imaging, and continuous monitoring. We are not aware of any direct negative societal impact specific to the method; it does not train any new large models, collect new data, or make deployment decisions itself.

RMEMSAFE contributes to an ongoing research program on *runtime safety signals for trustworthy machine learning*, where a model’s deployment-time behavior is gated by a quantitative reliability measure. Adjacent work in this program addresses out-of-distribution safety detection via typicality [1, 4, 5], grammar-based uncertainty quantification for LLMs in formal reasoning tasks [3, 6, 25, 26] and Hybrid reasoning and RAG systems [31, 33, 34]. RMEMSAFE contributes a third instance of the same design principle, specialized to the continual test-time adaptation regime: source-entropy-derived \mathcal{R}_{src} as a runtime gate on anchoring-based stability mechanisms, with the analytical graceful-decay guarantee of Proposition 1.

Intended use and positive impact. RMEMSAFE targets a specific safety failure mode in continual test-time adaptation: catastrophic anchoring to a frozen source that has itself collapsed under distribution shift. CTTA is increasingly deployed in settings where the input stream is non-stationary and labels are unavailable at test time, autonomous perception, medical imaging under acquisition drift, industrial monitoring, and in each of these the failure mode we diagnose (continuing to pull toward a $\sim 1\%$ -accurate reference at fixed strength) is a real deployment risk, not a benchmark artifact. The graceful-decay property of Proposition 1 is the safety contribution: when the source signal becomes uninformative, the source-coupled terms vanish rather than propagating a corrupted prior into the adapted parameters.

Risks of the method functioning correctly. The reliability gate uses source predictive entropy as its sole signal. This is sound for the high-entropy collapse regime (§3, App. P), but a confidently miscalibrated source, low entropy on wrong classes, is deemed reliable by \mathcal{R}_{src} and the anchor activates toward it. Standard CTTA benchmarks produce high-entropy collapse rather than low-entropy miscalibration, but deployment distributions need not. A practitioner who reads Proposition 1 as a general safety guarantee, rather than as a guarantee restricted to entropy-detectable failure, will misjudge when the method is protective. We flag this scope explicitly in §5 and recommend that high-stakes deployments pair the entropy gate with an independent correctness signal.

Risks of the method functioning incorrectly. On ViT-B/16 the entropy gate under-attenuates a confidently-wrong source ($\Delta = +1.14$ pp on the CCC mean, App. P) and the reset paradigm itself underperforms the non-reset baseline on CCC-Hard (§4.3). Both are characterized rather than fixed. A deployment using RMEMSAFE with a ViT backbone under severe shift should not assume the matched-split CCC gains transfer; the reliability-gated reset trigger of App. O partially addresses the second issue but is not a complete fix.

Misuse and dual-use. RMEMSAFE trains no new models, collects no data, and makes no deployment decisions on its own. We are not aware of a direct malicious-use pathway specific to this work beyond risks generic to robust-adaptation methods (e.g., a robust deployed system inherits whatever downstream uses its operator chooses).

Limitations.

1. **Scope of the reliability signal.** Entropy-only; does not detect confidently miscalibrated sources. ViT-B/16 under a class-permuted source is the empirical witness ($\Delta = +1.14$ pp, App. P).
2. **Reset-paradigm failure on CCC-Hard ViT-B/16.** Every reset-based method we evaluate underperforms non-reset ROID on this cell, across base adapters and reset mechanisms (§4.3). The reliability-gated reset trigger ($\tau_{\text{gate}} = 0.40$, App. O) recovers the non-reset mean but not per-split variance.
3. **Local-data offset on CCC.** Our shards yield CCC-Hard numbers ~ 7 pp harder than the streamed numbers of Lim et al. [14]; the offset is approximately constant across methods on ResNet-50. Cross-study absolute comparisons on CCC-Hard should be interpreted with caution; the matched-split head-to-head is the unbiased estimator of relative method quality.

4. **Fixed hyperparameters.** The five core hyperparameters are held constant across all nine benchmark cells. Per-cell tuning would likely yield further small gains but is discouraged in the unlabeled test-time setting.
5. **Marginal-calibration EMA under abrupt label shift.** The EMA prior ($\rho = 0.01$) lags abrupt label-distribution shifts; our streams exhibit gradual rather than abrupt shift, so this regime is not exercised.